



Dissolved organic matter characterization in soils and streams in a small coastal low-arctic catchment

5 Niek Jesse Speetjens¹, George Tanski^{1,2,3}, Victoria Martin⁴, Julia Wagner⁵, Andreas Richter⁴, Gustaf Hugelius⁵, Chris Boucher¹, Rachele Lodi⁶, Christian Knoblauch⁷, Boris P. Koch^{8,9}, Urban Wünsch¹⁰, Hugues Lantuit² and Jorien E. Vonk¹

¹Vrije Universiteit Amsterdam (VUA), Department of Earth Sciences, Earth and Climate Cluster, Amsterdam, 1081 HV Amsterdam, The Netherlands

²Alfred Wegener Institute (AWI) Helmholtz Centre for Polar and Marine Research, Permafrost Research Unit, 14473 Potsdam, Germany

10 ³Natural Resources Canada, Geological Survey of Canada–Atlantic, B2Y 4A2 Dartmouth, Canada

⁴University of Vienna (UniVie), Centre for Microbiology and Environmental Systems Science, Div. of Terrestrial Ecosystem Research, 1030 Wien, Austria

⁵Stockholm University (SU), Department of Physical Geography, 106 91 Stockholm, Sweden

15 ⁶Ca' Foscari University of Venice (Unive) and National Research Council, Institute of Polar Science (ISP-CNR), 30172 Mestre Venezia, Italy

⁷Universität Hamburg, Department of Earth Sciences, Institute of Soil Science, 20146 Hamburg, Germany

⁸Alfred Wegener Institute (AWI) Helmholtz Centre for Polar and Marine Research, Ecological Chemistry Research Unit, 27570 Bremerhaven, Germany

20 ⁹University of Applied Sciences, An der Karlstadt 8, 27568 Bremerhaven, Germany

¹⁰Technical University of Denmark, National Institute of Aquatic Resources, Section for Oceans and Arctic, 2800 Kgs. Lyngby, Denmark

Correspondence to: n.j.speetjens@vu.nl, niek.j.speetjens@gmail.com and j.e.vonk@vu.nl

25 **Abstract.** Ongoing climate warming in the western Canadian Arctic is leading to thawing of permafrost soils and subsequent mobilization of its organic matter pool. Part of this mobilized terrestrial organic matter enters the aquatic system as dissolved organic matter (DOM) and is laterally transported from land to sea. Mobilized organic matter is an important source of nutrients for ecosystems as it is available for microbial breakdown, and thus a source of greenhouse gases. We are beginning to understand spatial controls on the release of DOM as well as the quantities and fate of this material in large arctic rivers. Yet, these processes remain systematically understudied in small, high-arctic watersheds, despite the fact that these watersheds experience the strongest warming rates in comparison.

30



Here, we sampled soil (active layer and permafrost) and water (porewater and stream water) from a small catchment along the Yukon coast, Canada, during the summer of 2018. We assessed the organic carbon (OC) quantity (using dissolved (DOC) and particulate OC (POC) concentrations and soil OC content), quality ($\delta^{13}\text{C}$ -DOC, optical properties, source-apportionment), and bioavailability (incubations, optical indices such as slope ratio (Sr) and humification index (HIX)) along with stream water properties (T, pH, EC, water isotopes). We classify and compare different landscape units and their soil horizons that differ in microtopography and hydrological connectivity, giving rise to differences in drainage capacity.

Our results show that porewater DOC concentrations and yield reflect drainage patterns and waterlogged conditions in the watershed. DOC yield (in mg DOC g soil OC⁻¹) generally increases with depth but shows a large variability near the transition zone (around the permafrost table). Active layer porewater DOC generally is more labile than permafrost DOC, due to various reasons (heterogeneity, presence of a paleo-active layer, and sampling strategies). Despite these differences, the very long transport times of porewater DOC indicate that substantial processing occurs in soils prior to release into streams. Within the stream, DOC strongly dominates over POC, illustrated by DOC/POC ratios around 50, yet storm events decrease that ratio to around 5. Source-apportionment of stream DOC suggests a contribution of around 50 % from permafrost/deep-active layer OC, which contrasts to patterns observed in large arctic rivers (12 ± 8 % Wild et al., 2019). Our 10-day monitoring period demonstrated temporal DOC patterns on multiple scales (i.e. diurnal patterns, storm-events, and longer-term trend) underlining the need for high-resolution long-term monitoring. First estimates of Black Creek annual DOC (8.2 ± 6.4 t DOC yr⁻¹) and POC (0.21 ± 0.20 t yr⁻¹) export allowed us to make a rough up-scaling towards the entire Yukon Coastal Plain (34.51 ± 2.7 kt DOC yr⁻¹ and 8.93 ± 8.5 kt POC yr⁻¹). With raising arctic temperatures, increases in runoff, soil OM leaching, permafrost thawing and primary production are likely to increase the net lateral OC flux. Consequently, altered lateral fluxes may have strong impacts on the arctic aquatic ecosystems and arctic carbon cycling.

1. Introduction

Global temperatures are rising and due to arctic amplification, surface air temperatures in high latitudes have increased by more than double compared to the global average (Meredith et al., 2019). Through numerous feedback loops, these climatological changes have significant impacts on both arctic and global biogeochemical



60 cycles, climate and ecosystems (AMAP, 2017). Perennially frozen ground (permafrost), underlying about a 18 %
of the exposed land surface area in the northern hemisphere (Zhang et al., 1999, 2008), experiences significant
warming and thaw (Biskaborn et al., 2019; Olefeldt et al., 2016). This is likely to have far-reaching consequences
on local arctic ecosystems and communities (Teufel & Sushama, 2019) as well as globally through the permafrost
carbon feedback on global climate (Koven et al., 2011; MacDougall et al., 2012; Schuur et al., 2015).

65 Permafrost soils store large amounts of organic matter (OM) (Hugelius et al., 2014). The relatively flat ice-wedge
polygon (IWP) tundra plains, which are thought to cover around 2,600,000 km² (Mackay, 1972), or roughly ~12.4
% of the northern permafrost domain (Obu et al., 2019), are particularly rich in OC due to enhanced storage and
preservation of soil organic carbon (SOC) caused by waterlogged anaerobic conditions (Zimov et al., 2006, Fritz
70 et al., 2016). Upon thaw, microbial and physical decomposition of permafrost OM releases greenhouse gases
(GHG's). Thawing permafrost OM is released into aquatic systems as dissolved (DOM) and particulate organic
matter (POM), which have varying pathways in the ecosystem. While parts of the thawed permafrost OM (i.e.
carbon and nutrients) can be degraded quickly or directly incorporated into living organisms, the more refractory
parts can be mineralized over longer timescales or sequestered via sedimentation or burial (McGuire et al., 2009;
75 Huissteden & Dolman, 2012; Vonk & Gustafsson, 2013; Knoblauch et al., 2013). Little is known about the
controls on lateral permafrost OM release and transport pathways from soils to aquatic systems (Fouché et al.,
2017; Vonk, Tank & Walvoord, 2019; Beel et al., 2020; Coch et al., 2020). Hence it is challenging to assess
landscape-scale flux variability and integrated estimates of lateral carbon fluxes and budgets are scarce in these
permafrost landscapes. It is therefore a priority to better understand lateral permafrost carbon dynamics and their
80 biogeochemical implications for Arctic ecosystems on a landscape level in order to include them into future
projection models.

Most studies investigating lateral OM and nutrient fluxes in the Arctic focus on the largest Arctic rivers (Ob,
Yenisey, Lena, Kolyma, Mackenzie, Yukon), whose watersheds drain about two-thirds (~67 %) of the total Pan-
85 Arctic watershed area (16.8 10⁶ km²) (e.g. Mann et al., 2012; Holmes et al., 2012; Wild et al., 2019). While the
watersheds of the six largest rivers drain vast areas of land, only 35 % of their catchments are underlain by
continuous permafrost. In contrast, the eight next largest (“Middle 8”) and much smaller coastal catchments
draining to the Arctic Ocean (AO) are exclusively underlain by continuous permafrost (“Middle 8”: 60 %,
“Remainder”: 73 %) (Holmes et al., 2012). Smaller coastal watersheds experience a greater warming trend due to



90 their proximity to the coast where a rapidly-declining sea ice cover speeds up warming (Parmentier et al., 2013).
Despite this rapid warming and associated impacts on permafrost degradation (Olefeldt et al., 2016) and shifts in
hydrological and biogeochemical processes (Vonk et al., 2015), small watersheds remain understudied. Several
studies have however shown the relative importance of small watersheds in terms of discharge (e.g. Prowse &
Flegg, 2000; Lewis et al., 2010; Bring et al., 2016).

95

Permafrost DOM dynamics in small arctic watersheds are characterized by a high spatial and temporal variability
in terms of OM amount and composition and in terms of terrestrial imprint on stream DOM (e.g. Lewis et al.,
2012; Wauthy et al., 2018; Shatilla et al., 2019). Aquatic DOM fluxes are mainly driven by the underlying soil,
landform, climate and other environmental and chemical controls (Tank et al., 2020). Additionally, studies found
100 that land-ocean DOM fluxes in High Arctic watersheds are mainly controlled by thermal (active layer deepening)
and physical disturbances (e.g. retrogressive thaw slumps and thermoerosion) and increasingly impacted by
rainfall runoff instead of snowmelt (Beel et al., 2020; Lafrenière & Lamoureux, 2013). This is in good agreement
with studies in the western Canadian Arctic, where DOM fluxes increase (Coch et al., 2018) upon climate warming
and subsequent permafrost degradation. In contrast, there are also other studies suggesting a decrease in DOM
105 fluxes (e.g. Kawahigashi et al. 2004), resulting from increased mineral surface interaction as thaw depth increases
and disturbances become more frequent.

Here we focus on the Yukon coastal plain in the western Canadian Arctic (fig. 1), which is dominated by IWP
tundra with three IWP development stages: Low centered polygons (LCP), where ice wedges are large and intact,
110 high centered polygons (HCP), where ice wedges have already partially degraded, and flat polygons, which are
an intermediate stage in the transition from LCP to HCP (fig. 2). Wainwright et al. (2015) suggest that landscape-
scale classification by polygon type is useful in differentiating between lateral carbon flux magnitudes and
controls hence we follow this classification in differentiating soil characteristics. We targeted an unnamed creek
(referred to as Black Creek in this paper), draining a small IWP catchment (~ 4 km²). Our objectives are to quantify
115 and characterize stream water DOM and POM (main stem, and tributaries) as well as porewater DOM (different
thermal layers, soil horizons, and polygon types) within this catchment using a combination of bulk isotopic and
optical techniques. Additionally, we performed incubation experiments to assess the potential lability of soil and
stream OM. We also investigated landscape heterogeneity in terms of polygons types within a catchment as it
represents a gradient from water-logged, anoxic, stagnant conditions (LCP) to drained and aerated soil conditions



120 (HCP), and the imprints of LCP and HCP on the stream water outflow characteristics and OM flux. These
measurements present insights into the characteristics and dynamics of OM-release and controlling factors from
predominant landscape types that characterize circumpolar small coastal watersheds.

In summary, the aim of this study is to better assess the role of small circum-Arctic watersheds to improve our
125 current understanding of land-ocean OM budgets. The specific objectives of this study are to (i) characterize the
OM in the most dominant IWP types, (ii) investigate the degradation patterns of mobilized OM during transport
from soil to stream (i.e. bioavailability), (iii) determine the quantity, character and origin of OM exported from
the stream and ultimately (iv) to estimate the magnitude of annual OC exports from small streams on a landscape
scale. With this study, we provide valuable data on so far understudied small watersheds and help to build a
130 baseline, which allows for better estimates of panarctic land-ocean OM fluxes.

2 Materials and methods

2.1 Study Area

Black Creek Watershed (BCW) is situated on the Yukon coastal plain in the western Canadian Arctic and drains
into Ptarmigan Bay, which is a semi-open lagoon sheltered from the open Beaufort Sea (fig. 1). Black Creek is a
135 small coastal stream draining a polygonal tundra landscape underlain by continuous permafrost. The contributing
watershed area is approximately 4 km², estimated using ArcticDEM, a publicly available 10-meter resolution
digital elevation model (Morin et al., 2016; *accessed on May 28, 2020*), from which we obtained a watershed
delineation using GRASS GIS. The Yukon coastal plain stretches ~300 km from the Mackenzie Delta in the East
to the Alaskan border in the West. The Quaternary surficial geology is mainly characterized by lacustrine,
140 morainal, fluvial and colluvial deposits (Rampton, 1982). IWP tundra, moraine hills, wetlands, beaded streams
and thermokarst lakes are the predominant landscape types. The land cover can be classified as low shrub tundra,
subzone E (Walker et al., 2018) with occurrence of *Betula nana*, *Salix polaris*, mosses and lichens in HCP, while
graminoids dominate in LCP terrain. The mean summer temperature (June, July and August 1991-2020) is 7.7 °C
(± 4.6 °C) based on available data for three nearby stations (Herschel Island – Qikiqtaruk, Komakuk Beach and
145 Shingle Point). The mean annual temperatures at Shingle Point and Komakuk Beach are -9.9 °C and -11 °C
respectively and precipitation means 254 and 161 mm (Environment Canada,
https://climate.weather.gc.ca/climate_normals).



The region of interest is underlain by continuous permafrost and active layer depths average around 30–40 cm in
150 IWP terrain on nearby Herschel Island (Siewert et al., 2021). Ground ice volumetric content in the Yukon coastal
plain averages around 46 % but reaches as high as 74 % in some areas (Couture et al., 2018; Couture & Pollard,
2017). The warm season in the western Canadian Arctic, during which the stream network is active lasts
approximately four months (Dunton et al., 2006). On average the sea ice-break up in the southern Beaufort Sea
region starts around mid-May and freeze-up starts early October with prolonged open-water periods around the
155 Mackenzie delta area. Both, winter and summer sea ice extent and concentration gradually declined in recent
decades (Galley et al., 2016). The lengthening of the sea ice-free seasons leads to increased storm frequency and
intensity. In combination with higher surface temperatures in the region (Screen et al., 2012) these environmental
changes are expected to have a drastic impact on biogeochemical cycling and hydrological processes in the
western Canadian Arctic (Parmentier et al., 2017).

160 **2.2 Meteorological data**

During the sampling period (August 8th - 19th 2018), we collected on-site weather data at a 5-minute interval. Air
temperature was measured at 1.5 m above the ground (BTF11/002 TSic 506; ± 0.1 °C accuracy). Precipitation
was measured (Young Model 52203; 0.1 mm per tip; accuracy ± 2 %) at 0.5 m above the ground away from any
objects causing potential wind shadow. Wind speed was measured using Thies CLIMA (4.3519.00.173; ± 0.5 m
165 s⁻¹ accuracy). Available weather data from outside the sampling period was downloaded from the Canadian
Government Environment and Natural Resources website (<https://climate.weather.gc.ca>) for the three nearby
stations mentioned in 2.1 (Station ID: 2100636, 2100682 and 2100950 respectively).

2.3 Soil and water sampling and stream measurements

Soil and water samples were collected between the 9th and 19th of August 2018. Soil samples were taken at 46
170 sites within the main polygon types in the watershed (HCP, LCP and flat polygon), which were classified based
on field observations. Both, the active layer (AL) and upper permafrost (PF) were sampled. Active layer samples
of known field volume were collected from the main soil horizon types (O, A, B, Bf/Cf) and classified according
to Schoeneberger et al. (2012). Samples with visible gley or cryoturbation were marked additionally. Permafrost
samples were collected at 10 cm intervals below the permafrost table up to a depth of 100 cm from the surface
175 (subject to practicality) using either a steel pipe and sledgehammer, SIPRE corer or Hilti drill hammer. All soil



180 samples (AL and PF; $n = 153$) were stored frozen at $-18\text{ }^{\circ}\text{C}$ in zip-lock bags until further processing in the lab, where porewater extraction took place. Stream water samples were taken every six hours at the catchment outlet using an ISCO 3700 automatic water sampler (Teledyne). In addition, manual samples were taken along the main channel and at three tributary streams flowing into the main stem using pre-rinsed 500 mL Nalgene bottles, which were flushed with stream water three times prior to sampling. All water samples were filtered through pre-combusted and pre-weighed 47 mm glass fiber filters (GFF, Whatman, 47 mm diameter, $0.7\text{ }\mu\text{m}$ nominal pore size). Subsamples for DOC/ $\delta^{13}\text{C}$ -DOC analysis were acidified to $\text{pH} < 2.0$ using 36 % HCl (Suprapur) and stored cool ($4\text{ }^{\circ}\text{C}$) and dark. Subsamples for chromophoric and fluorescent DOM (CDOM/fDOM) were stored frozen and dark at $-18\text{ }^{\circ}\text{C}$. All filters with suspended material designated for total suspended solids (TSS), POC and POC- $\delta^{13}\text{C}$ analysis were stored frozen and dark. Basic hydro-chemical readings were taken at the stream outlet with an AP-5000 multiparameter probe (Aquaread), which was deployed at the catchment outlet from the 8th until the 19th of August. Measurements included relative water level (h [m]), water temperature (T [$^{\circ}\text{C}$]), acidity (pH), electrical conductivity (EC [$\mu\text{S m}^{-1}$]), turbidity [NTU], dissolved oxygen (DO [% saturation]), redox potential [mV] and CDOM abundance [$\mu\text{g L}^{-1}$]. The CDOM sensor was calibrated using a quinine sulfate equivalent solution (CDOM-CAL-600, Aquaread Ltd.) yet units are given in $\mu\text{g L}^{-1}$ as provided by the instrument. An empirical stage discharge equation was derived using flow measurements at different stages and fitting a quadratic function within the measured range to estimate discharge (Q [L s^{-1}]) as a function of the pressure head on the sensor (h [m]) of the stream (eq. 1).

195
$$Q = -21927h^2 + 7271.5h - 524.89 \quad (1)$$

The measurement was based on the creeks flowing cross-sectional area together with flow velocity (measured at 2/3 of the water depth and 25 cm increments using a M1 mini current meter and Z6 counting device (SEBA Hydrometrie GmbH & Co. KG)) at the outflow at varying water levels.

200 **2.4 Porewater extraction**

Frozen soil samples were wet weighed and slowly thawed at $8\text{ }^{\circ}\text{C}$. Porewater was then extracted from active layer and permafrost samples ($n = 142$) using Rhizon samplers (mean pore size of $0.6\text{ }\mu\text{m}$, Rhizosphere, Wageningen, The Netherlands) under cold and dark conditions in a cooler room ($4\text{ }^{\circ}\text{C}$). Subsamples for CDOM/fDOM analyses



205 were taken from the extracted porewater and transferred into 15 mL falcon tubes and stored frozen and dark until analysis. Subsamples for DOC/ $\delta^{13}\text{C}$ -DOC were acidified ($\text{pH} < 2$) and stored cool (at 4 °C) and dark in 40 mL pre-combusted glass vials until analysis.

2.5 DOC Concentration and Isotopes

210 The DOC concentration and $\delta^{13}\text{C}$ -DOC were measured with an Aurora 1030 DOC analyzer (OI Analytical, USA) connected via a Conflow V to an Isotopic Ratio Mass spectrometer (IRMS, Delta V, Thermo Scientific, Germany) at the University of Hamburg (Germany) (stream water incubation samples), the Alfred Wegener institute for Polar Research (Bremerhaven, Germany) (bulk porewater samples) following Hölemann et al. (2021) and at North Carolina State University (Raleigh, USA) (stream water bulk samples and porewater incubation samples). DOC concentrations were used to quantify the total amount of OC in a dissolved state within the watershed systems and $\delta^{13}\text{C}$ -DOC to derive the origin and relative degradation state of OM. DOC concentrations from porewater 215 were used to calculate yields in mg DOC g^{-1} soil dry weight and mg DOC g^{-1} soil organic carbon (SOC) using Eq. 2 and Eq. 3.

$$Y_{\text{soil}} = \frac{[\text{DOC}] \times m_w}{m_s \rho_w} \quad (2)$$

$$Y_C = \frac{[\text{DOC}] \times m_w}{m_C \rho_w} \quad (3)$$

220

Where m_w is the mass in grams of water present in the sample, measured as the difference of the bulk wet soil sample weight minus the dry weight and assuming the density of water at 4 °C as $\rho_w = 1 \cdot 10^3 \text{ g L}^{-1}$. m_s is the soil bulk dry weight and m_C is the total mass of SOC both in grams. SOC was measured as the fraction of the dry bulk weight lost on combustion at 550 °C multiplied by a conservative factor of 0.45 to convert from bulk soil organic matter (SOM) to SOC, in accordance with Jensen et al. (2018). 225

2.6 POC concentration and Isotopes

Carbonates were removed from freeze-dried filters using acid-treatment. For this, filters were subsampled (16 filter punches of 4 mm cross-section) into silver capsules, moisturized with 25 μL of distilled water, acidified with 25 μL of 1 M HCl and left for 30 minutes at room temperature. Then, 50 μL of HCl was added and samples



230 were dried in an oven for 3 hours at 60 °C. After that, silver capsules were folded and analyzed for % OC, % N, and $\delta^{13}\text{C}$ (‰ VPDB) at the Vrije Universiteit Stable Isotope Laboratory (Amsterdam, The Netherlands).

2.7 Stable water isotopes of stream and porewater samples

Deuterium and oxygen isotopes (δD and $\delta^{18}\text{O}$) were measured on water subsamples with a Continuous Flow Deltaplus X IRMS coupled to a Flash Elemental Analyzer and High Temperature Conversion Elemental Analyzer (TC/EA) at Vrije Universiteit Amsterdam and are given as ‰ difference from Vienna Standard Mean Ocean Water (VSMOW). Deuterium excess was used to allocate the precipitation source (e.g. Fritz et al., 2016) in the same region ($d\text{-excess} = \delta\text{D} - 8\delta^{18}\text{O}$; Fritz et al., 2016, Dansgaard, 1964). Data was compared with water isotopic values from two local meteoric water lines (LWML) in Inuvik (200 km south-east) ($\delta\text{D} = 7.3 * \delta^{18}\text{O} - 3.5$) (Fritz et al., 2016) and Utqiagvik (former Barrow), Alaska (600 km north-west) ($\delta\text{D} = 7.5 * \delta^{18}\text{O} - 1.1$) (Throckmorton et al., 2016).

2.8 DOM optical properties

The chromophoric fraction of DOM was used to characterize DOM and identify the source. The CDOM and fDOM (fluorescent DOM fraction) were used as indicators of DOM quality such as degradation status, molecular size, and DOM source (Stedmon & Nelson, 2015). We used a range of absorbance and fluorescence indices for characterization of DOM, summarized in Table 1. Fluorescence data was processed using drEEM toolbox (Murphy et al., 2013) in MATLAB (R2017b). CDOM and fDOM were measured on a Horiba Aqualog fluorescence spectrophotometer at the Technical University of Denmark (DTU, Copenhagen).

2.9 DOM lability

In this study we chose four indicators to estimate degradation state and to infer lability:

- 250
1. Slope ratio (S_r), calculated as the ration between the slope of the absorbance between 275–290 nm and 350–400 nm and absorbance ratio ($a_{254}:a_{365}$) have been recognized as indicators of DOM molecular weight (MW) (Helms et al., 2008). The assumption is that lower MW organic molecules will generally be more bioavailable;
 - 255 2. The specific UV absorbance at 254 nm divided by the DOC concentration has been identified as a proxy for DOM aromaticity (Weishaar et al., 2003). Fouché et al. (2020) show that high S_r (i.e. low



molecular weight) and low SUVA₂₅₄ (i.e. low aromaticity) together are indicative of higher lability of permafrost DOM;

260 3. The degradation status, which can be inferred from the Humification index (HIX), calculated as the area under the emission spectra 435–480 nm divided by the peak area 300–345 nm + 435–480 nm, at excitation wavelength 254 nm (Ohno, 2002). DOM degradation in soils is the processing of labile fresh organic products (e.g. sugars) to more chemically complex and less bioavailable forms (Balser, 2005). Hence, more degraded DOM will generally be less labile.

265 4. Freshness index (FRESH) calculated from emission intensity at 380 nm divided by the maximum emission intensity between 420 nm and 435 nm at excitation 310 nm (Parlanti et al., 2000; Wilson & Xenopoulos, 2009) and fluorescence index (FI) the ratio of emission intensity at wavelength 470 nm and 520 nm, at excitation wavelength 370 nm which indicate what proportion of DOM is likely to be fresh and microbially produced (McKnight et al., 2001; Cory et al., 2010) of microbial origin. The assumption is that small, fresh, microbial leachates (i.e. high FI and FRESH) correlate with higher DOM lability.

270

Additionally, we performed incubations with stream and porewater samples to estimate the degradation potential of DOC by comparing DOC concentrations and $\delta^{13}\text{C}$ -DOC values before and after incubations.

2.9.1 Stream water incubation

275 For three tributary streams three aliquots of 60 mL water were incubated (in the field) for 14 days at ambient air temperature of $\sim 4^\circ\text{C}$ under dark and oxygenated conditions in 120 mL amber glass vials. These incubations were repeated at three different instances during the field campaign. Samples were turned regularly to prevent flocculation and mimic mixing in the stream. Incubations were stopped after two (T=2), seven (T=7) and 14 days (T=14). At each time step, samples were filtered using pre-combusted glass fiber filters (GFF, nominal pore size 0.7 μm). The filtrate was split into subsamples for DOC/ $\delta^{13}\text{C}$ -DOC analysis (acidified to pH <2.0 with 36 % HCl
280 (Suprapur) and stored dark at 4°C), and subsamples for CDOM/fDOM (stored dark and frozen at -18°C).

2.9.2 Porewater incubation

We incubated porewater extracts from six upper active layer samples (Oi-horizon) and nine upper permafrost samples at the Vrije Universiteit in Amsterdam to check for differences in OM degradation potentials between active layer and permafrost. Incubations were conducted under laboratory conditions following procedures



285 adapted from Vonk et al. (2013) and Spencer et al. (2015). Rhizon-filtered samples (median pore size 0.6 μm)
were transferred to pre-combusted 40 mL amber glass vials, holding in total 30 mL of sample. An inoculum was
added and prepared from a soil slurry consisting of a total of 12 g (2 g of each) of the sampled Oi-horizons mixed
with 240 mL of autoclaved tap water. The slurry was filtered through a glass fibre filter (Whatman, 1.2 μm
nominal pore size) and 1 mL was added to each incubation sample. Samples were then placed on a shaker table
290 for incubations at 8 °C under dark and oxygenated conditions. The incubations were stopped after T=2, 7, 14 and
21 days by acidification to pH < 2.0 (using 36 % HCl, Suprapur). Samples were stored cool (4 °C) until further
analysis for DOC concentration and $\delta^{13}\text{C}$ -DOC.

2.10 Endmember mixing model

Along with isotope tracers such as $\delta^{13}\text{C}$ -DOC, $\Delta^{14}\text{C}$ -DOC, δD and $\delta^{18}\text{O}$ (Vonk et al., 2012; Grotheer et al., 2020),
295 absorbance and fluorescence properties have been successfully used for source apportionment approaches and to
characterize DOM and trace sources (Lee et al., 2020). We used Endmember Mixing Model Analysis (EMMA)
to estimate the contribution of three potential sources (permafrost, active layer, and in-stream primary production)
to the Black Creek stream using $\delta^{13}\text{C}$ -DOC, Sr and a_{254}/a_{365} as tracers. These parameters are considered semi-
conservative and most distinctive in separating endmembers. We used a Bayesian mass-balance source
300 apportionment model with Metropolis-Hastings Markov Chain Monte Carlo sampling following Bosch et al.
(2015) in MATLAB R2017b. To compute source contributions, we ran the model with a time series of measured
 $\delta^{13}\text{C}$ -DOC, Sr and a_{254}/a_{365} at the catchment outlet over time. Although sample size is limited due to practical
limitations, we chose to use $\delta^{13}\text{C}$ -DOC of porewater instead of $\delta^{13}\text{C}$ -SOC of soils to avoid fractionation effects
from soil-to-water leaching (e.g. Kaiser et al., 2001; Boström et al., 2007) impacting the source-apportionment.
305 For active layer, we used a $\delta^{13}\text{C}$ -DOC value of -26.4 ± 1.07 ‰ based on the porewater DOC- $\delta^{13}\text{C}$ measurements
in the catchment (n = 3). Active layer values for Sr and a_{254}/a_{365} were also based on porewater samples from the
catchment and were 0.71 ± 0.08 (n = 45) and 4.55 ± 0.8 (n = 45), respectively. For permafrost we used a $\delta^{13}\text{C}$ -DOC
value of -24.15 ± 1.03 ‰ (n = 6), and Sr and a_{254}/a_{365} of 0.85 ± 0.08 (n = 44) and 5.81 ± 1.2 (n = 45) respectively,
based on $\delta^{13}\text{C}$ -DOC and Sr and a_{254}/a_{365} of permafrost porewater. Finally, the primary production source was
310 set to -28.48 ± 1.0 ‰ (n = 9) based on $\delta^{13}\text{C}$ -DOC values of the tributaries where we observed primary production
(algal mats). The standard deviation of the analyzed endmember samples was 0.237 ‰. However, we
acknowledge that the tributary water $\delta^{13}\text{C}$ -DOC signal probably consists of a mixture of terrestrial and primary



production source leachates. Moreover, it is likely that fractionation takes place during leaching from OM sources, including primary production sources. Hence, we expect a pure primary production signal would be more depleted than that found in the tributary water and we have therefore increased the standard deviation to ± 1 ‰, similar to the other $\delta^{13}\text{C}$ -DOC sources, to account for uncertainty. The Sr and a_{254}/a_{365} of the primary production endmember were set at 0.78 ± 0.020 ($n = 9$) and 5.40 ± 0.23 ($n = 9$) respectively. To estimate mixing with terrestrial DOC we also ran the simulation with $\delta^{13}\text{C}$ -POC (32.68 ± 2.00 ‰, $n = 9$) instead of $\delta^{13}\text{C}$ -DOC by means of sensitivity analysis. We acknowledge that using the $\delta^{13}\text{C}$ -POC to trace DOM is not incorporating potential fractionation efforts through leaching and that the most realistic primary production $\delta^{13}\text{C}$ value probably lies between the $\delta^{13}\text{C}$ -DOC and $\delta^{13}\text{C}$ -POC values used here.

We performed a sensitivity analysis by increasing and decreasing (± 5 %) permafrost endmember tracer means and standard deviations separately and comparing the effect (percentage change) on relative contribution of each source in the mixing model. The sensitivity analysis focused on permafrost endmember values since we are primarily interested in the relative contribution of thawing permafrost. Additionally, it is assumed that changing other endmember tracer mean and standard deviation by the same order of magnitude will result in same order of magnitude changes in relative source contribution and testing with only permafrost is representative of all endmembers.

2.11 Statistical analyses

All statistical analyses were performed in Python 3 programming environment (Van Rossum & Drake, 2009) using pandas (McKinney, 2010), scipy (Jones et al., 2015) and statsmodels (Seabold & Perktold, 2010) packages. Significance statistics were calculated with a two-sided T-test. Linear regression results were obtained using linear least-squares regression for two sets of measurements as described in the scipy manual.

3 Results

3.1 Meteorology and hydro-geochemistry

Weather conditions during the field campaign were variable with air temperatures ranging between -0.8 °C and 12.7 °C (*mean*: 4.2 ± 2.6 °C) (fig. S1). The predominant wind direction was northwest with mean wind speeds of 4.78 ± 2.92 m s⁻¹ and gusts up to 15.1 m s⁻¹ (7 Bft). Precipitation was generally low with notable rainfall recorded



340 on August 13 (1.3 mm) and between August 16 and 19 (7.7 mm cumulative). Total precipitation during the
monitoring period was 9.8 mm (table S1). Mean electrical conductivity (EC) at the catchment outlet was 954 μS
 cm^{-1} , pH ranged between 6.5 and 7.8 ($mean = 6.9 \pm 0.19$) and water temperature ranged between 2.9 °C and 12.3
°C ($mean = 6.6 \pm 1.7$ °C). During a storm event on the 16th and 17th of August water levels at the outlet monitoring
station peaked together with EC (19134 $\mu\text{S cm}^{-1}$). Discharge in the creek main channel showed a decreasing trend
345 ($min = 9$, $max = 140$, $mean = 43 \pm 27$ L s^{-1}) during the measurement period. Discharge during the storm event of
the 16th and 17th was disregarded due to uncertainty regarding tidal influence, which is indicated by the elevated
EC values. Water isotope values within the main channel ranged between -130.3 ‰ and -127.1 ‰ (δD) and -16.35
‰ and -16.25 ‰ ($\delta^{18}\text{O}$) with mean values of -128.0 ± 1.2 ‰ and 16.32 ± 0.03 ‰ respectively. In tributary streams
stable water isotope values covered a wider range, between -132.4 ‰ and -94.38 ‰ (δD) and -17.11‰ and -
350 11.94‰ ($\delta^{18}\text{O}$) with mean values of -122.9 ± 7.5 ‰ and 15.71 ± 0.98 ‰, respectively. Stable water isotope signals
were grouped by main source (i.e. permafrost and active layer porewater, tributaries, main channel) (table 2). The
correlation of δD and $\delta^{18}\text{O}$ for the samples compared to the local meteoric water line (LMWL) in Inuvik shows
that permafrost samples group in roughly three lines that are distinguished by their d-excess (fig. S2). The majority
of the permafrost samples plot further from the LMWL at Inuvik than the modern samples (streams and active
355 layer), which in turn also are deviating from the Inuvik LMWL.

3.2 OC concentrations and stable isotopes

3.2.1 Concentrations and $\delta^{13}\text{C}$ of DOC and POC in streams

The DOC concentrations in the main channel upstream and at the outlet were on average 13.3 ± 2.04 mg L^{-1} and
 16.0 ± 3.25 mg L^{-1} , respectively (fig. 3, table S2). At the outlet, values below 5 mg L^{-1} were measured during the
360 storm event of August 16th and 17th. DOC concentrations correlated with measured CDOM (Aquaread's
Aquaprobe AP-5000) concentrations (133.7 ± 29.02 $\mu\text{g L}^{-1}$; fig. 3, table S2), and showed a gently declining trend
over the monitoring period. The average DOC concentrations measured in tributaries were significantly higher (p
< 0.05) (22.74 ± 8.66 mg L^{-1}) than in the main stem. POC concentrations and $\delta^{13}\text{C}$ -POC values in the main channel
(0.41 ± 0.2 mg L^{-1} , -29.31 ± 0.829 ‰) were significantly different ($p < 0.05$) to the values in the tributary streams
365 (1.16 ± 0.604 mg L^{-1} , -32.68 ± 2.042 ‰, Table 3). The POC concentrations increased during the storm event,
opposite to DOC concentrations which declined. Similarly, during this event the $\delta^{13}\text{C}$ -POC signal became less
depleted whereas the $\delta^{13}\text{C}$ -DOC signal became slightly more depleted. The tributaries had the most depleted $\delta^{13}\text{C}$ -



DOC signal (-28.476 ± 0.2368 ‰) of all samples. In the tributaries we observed algal production. The $\delta^{13}\text{C}$ -POC signal of the filters taken from this tributary were the most depleted found during this study (-35.25 ± 1.00 ‰, $n=3$).

3.2.2 Concentrations, yields, and $\delta^{13}\text{C}$ of DOC and SOC in soils

SOC contents (% of dry weight) of the sampled soils were high but differed strongly (fig. S3, table S3) between LCP active layer (26 ± 13.2 %, $n = 16$) and LCP permafrost (17 ± 10.7 %, $n = 21$) while differences for HCP active layer (23 ± 12.8 %, $n = 38$) and HCP permafrost (18 ± 6.2 %, $n = 44$) as well as flat active layer (17 ± 13.5 %, $n = 12$) and flat terrain permafrost (15 ± 7.7 %, $n = 11$) were less pronounced. Differences between permafrost and active layer were significant between LCP and HCP classes ($p < 0.05$) but not for flat type polygons. Although the differences between the three landscape classes within each thermal layer were large, they were not significant ($p > 0.05$).

The DOC concentration in porewater extracts showed a great variability (142.3 ± 83.62 mg L⁻¹) but were significantly ($p < 0.05$) higher in permafrost (181.3 ± 82.86 mg L⁻¹) compared to the active layer extracts (88.96 ± 47.55 mg L⁻¹). Among permafrost samples, a significant concentration difference was found between HCP (171.19 ± 87.8 mg L⁻¹) and LCP (150.61 ± 63.1 mg L⁻¹) as well as HCP and flat (146.26 ± 89.5 mg L⁻¹) type polygons ($p < 0.05$) with HCP having the highest concentrations (fig. 4a). Active layer DOC concentrations were not significantly different between polygon types.

DOC yields (Fig. 4c,d) were highly variable both in permafrost (0.27 ± 0.27 mg g⁻¹ soil, 2.10 ± 2.65 mg g⁻¹ C) and active layer soils (0.22 ± 0.31 mg g⁻¹ soil, 2.97 ± 6.69 mg g⁻¹ C), but were not significantly different from each other. While permafrost DOC yield is higher at lower SOC content, active layer DOC yield is highest with higher SOC (fig. 4c,d). Results also show that gleyed soils have slightly higher DOC yield (2.54 ± 1.82 mg g⁻¹ C) compared to other active layer samples (2.31 ± 1.85 mg g⁻¹ C). DOC yields above 7.10 mg DOC g⁻¹ C were considered as outliers since they were not within the 95-percentile range and therefore removed from the yield analyses. The DOC yields of permafrost samples are generally increasing with depth. Although DOC concentrations were significantly different ($p < 0.05$) between permafrost and active layer samples as well as between HCP permafrost and LCP permafrost, DOC yields were similar among the different classes (fig. S4).



This is similar for DOC concentrations which were not significantly different ($p > 0.05$) between polygon types in the active layer.

The $\delta^{13}\text{C}$ -DOC values varied significantly ($p < 0.05$) between most sample sources. Values were highest and most variable in HCP permafrost (-23.68 ± 1.2 ‰) followed by LCP permafrost (-25.05 ± 0.5 ‰). LCP permafrost $\delta^{13}\text{C}$ -DOC was not significantly different ($p = 0.0519$) from the $\delta^{13}\text{C}$ -DOC signal in the main channel (-25.40 ± 0.4 ‰). In contrast to that, the $\delta^{13}\text{C}$ -DOC signature in HCP active layer was more depleted and had a wider range (-26.38 ± 1.1 ‰). The SOC- $\delta^{13}\text{C}$ values in the catchment were generally more depleted than porewater $\delta^{13}\text{C}$ -DOC (table 3); for permafrost and active layer in HCP (PF: -26.91 ± 1.0624 ‰, AL: -27.41 ± 0.9 ‰), LCP (PF: -27.01 ± 1.0 ‰, AL: -28.27 ± 1.0 ‰) and flat (PF: -27.73 ± 0.9 ‰, AL: -27.93 ± 0.9 ‰). The difference between porewater $\delta^{13}\text{C}$ -DOC and soil $\delta^{13}\text{C}$ -SOC is larger for permafrost (LCP: 2.25 ‰, HCP: 3.7 ‰) compared to active layer (HCP: 1.21 ‰, LCP: n/a (tables S3 and S4).

3.3 Degradability of DOC

Incubation experiments show a high variability in DOC loss as well as $\delta^{13}\text{C}$ -shifts for active layer and permafrost (fig. 5). The degradability of DOC strongly differed between samples. The mean loss of DOC [%] from incubations with water from the three different tributary locations (A, B and C) was 4.30 ± 5.3 % after 7 days of incubation. During this period, mean isotopic values of $\delta^{13}\text{C}$ -DOC did not change significantly ($p > 0.05$) (-28.48 ± 0.2 ‰ at $T = 0$ days and -28.52 ± 0.3 ‰ at $T = 7$ days). However, looking at individual samples, $\delta^{13}\text{C}$ -DOC enrichment was observed in several cases (table S3, fig. S5). Location A and B showed comparable patterns with depletion of $\delta^{13}\text{C}$ in the first 7 days and repletion between day 7 to 14, location C showed almost a linear trend toward a less depleted $\delta^{13}\text{C}$ -DOC signal over time. The incubation of porewater showed that DOC losses are in the same range as the tributaries and that there are no significant differences between HCP permafrost (5.0 ± 6 % DOC loss, $n = 3$, $T = 7$ days) and LCP permafrost (7.0 ± 1 % DOC loss, $n = 2$, $T = 7$ days) ($p > 0.05$). In contrast to that, active layer DOC from concentration the Oi-horizon, although much lower in, showed significantly higher relative DOC losses (17.3 ± 16 %, $n = 3$, $T = 7$ days). The $\delta^{13}\text{C}$ -DOC signals are significantly different between active layer, LCP permafrost and HCP permafrost at the begin of the incubation ($T=0$) and, on average, become



slightly more enriched over time. Yet, there is no significant change in $\delta^{13}\text{C}$ -DOC between T=0 and T=21 (table 4, fig. S6).

3.4 Optical properties of DOM in the catchment

425 Values of SUVA_{254} at the catchment outlet varied between ~ 1.71 and $\sim 11.73 \text{ L mg}^{-1} \text{ C m}^{-1}$ and averaged around
 $\sim 3.68 \pm 2.3 \text{ L mg}^{-1} \text{ C m}^{-1}$ ($n = 27$). The highest values of SUVA_{254} correspond with low concentrations of DOC
during the storm event (August 16th and 17th). With exclusion of these storm event extremes, mean SUVA_{254}
values were slightly lower ($\sim 3.07 \pm 0.5 \text{ L mg}^{-1} \text{ C m}^{-1}$) and not significantly ($p > 0.05$) different from mean SUVA_{254}
430 values in tributaries ($\sim 3.86 \pm 1.8 \text{ L mg}^{-1} \text{ C m}^{-1}$). Permafrost porewater showed significantly lower SUVA_{254} (~ 1.00
 $\pm 0.6 \text{ L mg}^{-1} \text{ C m}^{-1}$) ($p < 0.05$) than active layer porewater ($\sim 2.13 \pm 0.9 \text{ L mg}^{-1} \text{ C m}^{-1}$). Highest mean active layer
porewater SUVA_{254} is found in HCP ($\sim 2.4 \pm 0.9 \text{ L mg}^{-1} \text{ C m}^{-1}$) followed by flat ($\sim 2.14 \pm 0.9 \text{ L mg}^{-1} \text{ C m}^{-1}$) and
LCP ($\sim 1.55 \pm 1.1 \text{ L mg}^{-1} \text{ C m}^{-1}$). For permafrost the order was different, HCP showing the lowest values for
 SUVA_{254} ($\sim 0.91 \pm 0.7 \text{ L mg}^{-1} \text{ C m}^{-1}$) followed by LCP ($\sim 1.06 \pm 0.6 \text{ L mg}^{-1} \text{ C m}^{-1}$) and flat polygon type showing
435 highest SUVA_{254} ($\sim 1.23 \pm 0.6 \text{ L mg}^{-1} \text{ C m}^{-1}$) in permafrost. Slope ratio (Sr), which negatively correlates with MW
of DOM, was negatively correlated with SUVA_{254} in our porewater samples while Sr shows a weak positive
correlation with SUVA_{254} (i.e. lower MW molecules were less aromatic). In stream water samples, however, Sr
was positively correlated with SUVA_{254} (i.e. lower MW molecules were more aromatic). For fluorescence index
and biological index (FI, BIX), which are used to indicate terrestrial sources of DOM (i.e. soil organic matter and
plant litter/low FI and BIX) and relatively fresh, more microbially-derived DOM (i.e. leachates and products of
440 algae and bacteria/high FI and BIX) (Fouché et al., 2017) the same holds: in porewater samples the aromaticity
was highest in samples with a terrestrial and less fresh DOM signal, while in streams the aromaticity was highest
in samples with relatively fresh DOM signal.

Overall, our results show a predominantly terrestrial signature in streams which is slightly but significantly ($p <$
445 0.05) higher in tributaries (FI: ~ 1.47 , BIX: ~ 0.50 , Sr: ~ 0.80) compared to the outlet (FI: ~ 1.49 , BIX: ~ 0.55 , Sr:
 ~ 0.85). This signal is comparable to that of porewater in the active layer (FI: ~ 1.46 , BIX: ~ 0.48 , Sr: ~ 0.81). In
contrast, the permafrost porewater averages around a more fresh, microbial and lower MW signature (FI: ~ 1.65 ,
BIX: ~ 0.62 , Sr: ~ 0.93). Permafrost and active layer are significantly different with respect to their SUVA_{254} , FI,
BIX, and Sr values ($p < 0.05$). However, when looking closer at the distribution of their values within the soil
450 profile, we observe linear trends with depth respective to the permafrost table rather than clustering linked



explicitly to each thermal layer (fig. S7). With respect to polygon types, results show that HCP-active layer spectral indices are significantly different ($p < 0.05$) from the other polygon classes except for HIX and that differences between active layer and permafrost are most pronounced in HCP (table S6, fig. 6). The humification index (HIX) peaks in HCP active layer (~ 0.86), while lowest HIX was found in HCP permafrost (~ 0.75) (table 5). A more detailed peak in HIX around the permafrost table suggests the prevalence of more degraded SOM (fig. S7). With deeper permafrost sampling depth, a decreasing HIX value is observed. Although distinctly different, values of HIX are neither significantly different between active layer and permafrost nor between landscape classes. Values of HIX were highest in streams (~ 0.95) and the active layer (~ 0.85).

3.5 Endmember-based source apportionment of DOM

With our initial source apportionment setup, we modelled source contribution with mean isotopic (fig. S8) and spectral index values at the outlet ($\delta^{13}\text{C-DOC}$: -25.40 ‰, a_{254}/a_{365} : 5.55 and Sr: 0.86) for three endmembers (Permafrost OM, Active layer OM and primary production OM). Model results given these inputs indicate a relative contribution of these sources of $\sim 48 \pm 20$ %, $\sim 30 \pm 21$ % and $\sim 22 \pm 15$ % respectively (table 6, fig. S9, S10). We used the maximum (-26.08 ‰) and minimum (-24.73 ‰) $\delta^{13}\text{C-DOC}$ values and corresponding Sr and a_{254}/a_{365} at the outlet to assess variation of source contribution over time. Correspondingly, we find that permafrost, active layer and primary production OM contributions vary with between 31-67 %, 20-38 % and 14-31 % respectively. When calculating the source apportionment considering HCP permafrost and LCP permafrost as different DOM sources (HCP permafrost $\delta^{13}\text{C-DOC}$: -23.68 ± 1.2 ‰, Sr: 0.94 ± 0.1 , a_{254}/a_{365} : 6.08 ± 1.1 and LCP permafrost $\delta^{13}\text{C-DOC}$: -25.05 ± 0.5 ‰, Sr: 0.92 ± 0.01 , a_{254}/a_{365} : 5.67 ± 1.4), the mean relative contribution of permafrost sources increases from 48 % to 58 % at the catchment outlet. When using $\delta^{13}\text{C-POC}$ of the primary production sources instead of $\delta^{13}\text{C-DOC}$, this leads to a decrease in primary production contribution from 21 % to 11 %, mostly resulting in an increase of permafrost contribution from 48 % to 55 % and an increase of active layer contribution from 31 % to 34 % (table 6 and 7). A summary of the time series and computed source contributions using $\delta^{13}\text{C-DOC}$ of primary production can be found in table S9.

From sensitivity analysis (i.e. changing input parameters with fixed relative amounts) we observed that modelled source contributions respond strongest to shifts in $\delta^{13}\text{C-DOC}$. When decreasing the permafrost mean $\delta^{13}\text{C-DOC}$ from -24.15 ‰ to -25.36 ‰, this resulted in a shift from 49 % to 52 % of relative contribution while active layer



480 contribution remains constant and primary production decreases from 21 % to 17 %. Inversely, when using a higher permafrost mean $\delta^{13}\text{C}$ -DOC (-24.15 ‰ to -22.94 ‰) this results in a decrease of its contribution from 49 % to 40 % while primary production increased from 21 % to 27 % (table S7 and S8) and active layer increased from 31 % to 33 %. Changing standard deviations of permafrost endmember values by ± 5 % leads to changes in contribution ranging from - 3 % for permafrost to + 5 % for primary production.

4 Discussion

485 The aim of this study is to better assess the role of small circum-Arctic watersheds to improve land-ocean OM budgets. The specific objectives of this study are to (i) characterize the OM in the most dominant IWP types (4.1), (ii) investigate the degradation patterns of mobilized OM during transport from soil to stream (4.2), (iii) determine the quantity, character and origin of OM exported from the stream (4.3) and ultimately (iv) to estimate an annual OC export from small streams on a landscape scale (4.4).

490 4.1 Differences of OM pools in HCP and LCP

Our data show that there are significant differences in terms of their OM pools between the two thermal layers (i.e. active layer and permafrost) and between the main landscape features that define the terrain (i.e. HCP and LCP). The main differences between HCP and LCP are the micro-topography and hydrological pathways, which may influence OC characteristics. The wetter soils in LCP have higher thermal conductance, hence summer active layer depths in the center of the polygon often reach deeper than in HCP (Liljedahl et al., 2016, Walvoord & Kurylyk, 2016, Wales et al., 2020). LCP's elevated ice wedge rims generally promote waterlogged conditions in the polygon center while in HCPs, the degraded ice wedges form connected drainage channels resulting in well drained polygon centers (Liljedahl et al., 2012).

500 Differences in drainage patterns are reflected in our observed DOC concentrations and yields. Mean SOC contents are higher in the active layer (LCP: 26 ± 13.2 %, HCP: 23 ± 12.8 %) compared to the permafrost (LCP: 17 ± 10.7 %, HCP: 18 ± 6.2 %). This contrasts with the DOC concentrations, which are higher in permafrost (HCP: 171.20 ± 87.8 mg L⁻¹, LCP: 150.62 ± 63.1 mg L⁻¹) compared to active layer (HCP: 95.20 ± 53.7 mg L⁻¹, LCP: 92.98 ± 53.2 mg L⁻¹). The high mean DOC concentrations in permafrost porewater (162.44 ± 82.0 mg L⁻¹) compared to those of active layer (97.14 ± 52.54 mg L⁻¹) indicate that the permafrost DOC pool is still freeze-locked (i.e. immobile)



510 whereas the active layer has been flushed more regularly. Differences in DOC concentration between active layer and permafrost were highest in HCP and lower in the LCP polygon type category. This could indicate that in the active layer of HCPs, DOM was already subject to more degradation and flushing with runoff. This is also suggested in a simulation study by Liljedahl et al. (2012) showing that in LCP terrain 46 % of the snow water equivalent was flushed as runoff while this was 73 % in HCP terrain.

515 Overall our data show a trend of increasing DOC yield ($\text{mg DOC g}^{-1} \text{SOC}$) with increasing depth in the soil. The depth below the permafrost table showed to be a good indicator of DOC concentration as well ($[DOC] = 2.028 \cdot \Delta z_p + 134.60, R^2 = 0.71, p = 8.6e^{-37}$). The SOC-content showed a negative correlation with depth (fig. 7), dipping around the permafrost table. This ‘dipping’ effect could be ascribed to the increasing likelihood of waterlogging conditions to occur near the permafrost table of HCP soils (Harden et al., 2012). Signs of stagnant water were observed in several gleyed (typical brown/orange to grey/blueish colour patterning caused by waterlogged anoxic conditions) soil profiles. We also noted that in gleyed soil samples, comprising mostly mineral soils (B-horizons), there often was a low SOC content relative to the DOC concentration (i.e. a high DOC yield in mg-DOC/g C).
520 This suggests that these soils, due to their waterlogged conditions, are either efficiently leached out and/or DOC is flushed in from overlaying O-horizons and accumulates. The $\delta^{13}\text{C}$ signature of DOC shows a more degraded (i.e. more enriched) signal than the bulk SOC- $\delta^{13}\text{C}$, indicating that the degraded fraction of SOM is preferably leached and/or sorption processes are affecting $\delta^{13}\text{C}$ -DOC signatures. Moreover, we find that values of permafrost $\delta^{13}\text{C}$ -DOC are more enriched than those of active layer, indicating a more processed OM pool, or a stronger DOC
525 leaching effect on ^{13}C in mineral permafrost horizons than organic surface horizons.

4.2 Mobilization and degradation dynamics of OM from soils to streams

Our incubation experiments suggest that active layer DOC shows a higher lability (17 % DOC loss in 7 days) than DOC found in permafrost (HCP: 5 % DOC loss, LCP 7 % DOC loss in 7 days). In a meta-analysis, Vonk et al.,
530 (2015) calculated average bio-labile DOC (BDOC) content in permafrost of ~16 % after 28 days of aerobic incubation ($T = 15\text{-}25\text{ }^\circ\text{C}$, $n = 205$) and even higher BDOC content when looking at continuous permafrost zone leachates only, based on several studies. Although our incubations were done at lower temperatures ($4\text{ }^\circ\text{C}$), we observed that degradation rates stagnated after ~14 days, hinting that most labile BDOC would have been processed by then. Selvam et al. (2017), who incubated permafrost peat, showed much lower lability (~3 % after
535 7 days), which confirms that the bioavailability of DOM in permafrost is variable. It is worth noting that the



540

maximum depth at which permafrost was sampled in the study by Selvam et al. (2017) was only 5 cm below the permafrost table, comparable to our study. Vonk et al., (2015) could not include depth in their assessment of permafrost DOM lability due to limitations in the data. However, they do acknowledge the linkage between depth and DOM character and showed highest lability in deep Yedoma layers. In the following paragraphs we present several explanations for the bioavailability of our samples.

4.2.1 Low DOC concentration with high bioavailability in the upper active layer

545

Our results show high variability in OM composition and quantity within the active layer. This is reflected in the DOC concentrations as well as the variability of its spectral properties. Oi-horizons in HCP showed relatively high SOC content and low DOC concentrations. We interpret this as a high abundance of fresh plant material, which leaches less than more degraded plant material. Fresh DOM consists primarily of bioavailable sugars and products of microbial activity such as amino acids (Balsler, 2005) which could explain why our Oi-DOM incubations showed relatively high BDOC loss compared to permafrost samples.

4.2.2 Inversed degradation status with depth in permafrost

550

More degraded DOM contains more humic-like substances (Ohno, 2002). Hence, as is expected in soil profiles, an increasing degradation status with depth is reflected in our results (fig. S7). We see a (weak) increasing trend in HIX (i.e. higher ratio of humic-like substances to protein-like substances) with depth in the active layer. The elevated HIX values continue into the upper permafrost, but start decreasing again with greater depth (>~20 cm) within the permafrost. An explanation is be the presence of a transition layer and/or paleo-active layer. During the Holocene thermal maximum (HTM) (~10.6 cal ka. BP) active layer depths reached a depth of at least twice the modern depth (Fritz et al., 2012; Fouché et al. 2020) implicating that the current permafrost may have been active layer in the past. This, together with interannual variability of maximum thaw depth explains why shallow permafrost bioavailability (and DOM composition in general) resembles that of the deep active layer more than anything (i.e. it has already undergone several periods processing and influx of soil water). More “untouched” bioavailable and less degraded OM is found deeper in the permafrost, where we had no incubation samples.

555

560

4.2.3 Bias through sampling depth and horizon limitations

Our sampling was limited by practical constraints in the field: permafrost cores from which we could extract sufficient pore water to perform incubation are from relatively shallow depths (~10 to 50 cm below permafrost



table, taken with a SIPRE corer), whereas smaller samples that were used for DOM spectral characterization reached greater depths (~10 to 100 cm below permafrost table, taken with a steel tube and sledgehammer). These deeper samples indicate increasing bioavailability with depth (e.g. fresh, low MW, low HIX, low aromatic DOM), however we could not confirm this with incubation experiments on the same samples.

4.2.4 Pre-incubation DOC losses

The spectral signatures of our DOM samples hint toward rapid processing upon thaw. As samples are thawed and prepared for porewater extraction it is inevitable that microbial activity starts up as well. The fact that we measure relatively low BDOC in permafrost DOM incubations but a clear signal of degraded DOM in samples at similar depths could mean that this permafrost DOM is indeed very labile. That would mean most of the BDOC is already lost in the first 24 hours before we extracted the water and is thereby missed by our measurements.

4.2.5 Translation of laboratory measurements to soil DOM dynamics in the field

It is difficult to accurately assess degradability and fate of DOM upon thaw, yet various studies have attempted tackling the problem of quantifying carbon fluxes from degrading permafrost landscape in in-situ (e.g. Schuur et al., 2009; Natali et al., 2014; Plaza et al., 2019), bulk soil incubation (e.g. Dutta et al., 2006; Lee et al., 2012; Gentsch et al., 2018) and lateral flux specific experiments (e.g. Kalbitz et al., 2003; Kawahigashi et al., 2006; Vonk et al., 2013, 2015). Porewater DOM incubation experiments as performed in this study are rare, however most confirm that DOM character and thus lability is highly variable on spatial scales (e.g. Shirokova et al., 2019; Fouché et al., 2020; MacDonald et al., 2021). Our results fall within the range of what is found in other studies (Vonk et al., 2015; Selvam et al., 2017) but are on average rather low for permafrost compared with active layer due to the reasons highlighted above. Nevertheless, our results show that DOM from, both, permafrost and active layer will likely be degraded within the soil. A relatively small proportion of the total SOM pool enters the aquatic system as DOM. Depending on transport times that DOM has undergone significant processing by the time it reaches the ponds, IWP troughs and headwater streams. Although small compared to the soil organic matter stock, the aquatic DOM ‘stock’ we observe in streams is predominantly terrestrially derived and high in aromatic, degraded components.



4.3 Stream water OM dynamics and drivers during the warm season

The OC export from our investigated watershed is dominated by DOC (mean_{DOC} : mean_{POC} = 16.03 mg L⁻¹ : 0.41 mg L⁻¹). This may be explained by the flat topography in this area which minimizes impacts of bank and thermo-erosion that enhance sediment mobilization (Costard et al., 2003), along with long residence times of ground water within the soil facilitating DOC leaching (Connolly et al., 2018). Similar dominances of DOC have been shown elsewhere in the panarctic watershed, both in large and small rivers (e.g. Holmes et al., 2012; Fabre et al., 2019; Coch et al., 2020) but this dominance may be even more pronounced for low-relief tundra plains. Based on satellite imagery (WorldView-2, DigitalGlobe Inc., acquired on July 18, 2018) an estimated ~ 80 % to ~ 90 % of our watershed consists of HCP terrain. The $\delta^{13}\text{C}$ -DOC and $\delta^{13}\text{C}$ -POC signatures from the stream water at the outlet compared to what was found in porewaters suggest that DOC is predominantly derived from HCP terrestrial sources (Mann et al., 2015) whereas POC likely stems from primary production of phytoplankton growth within the stream network or ice wedge troughs (Tank et al., 2011) or fragments of sedge biomass transported into the stream (Wooller et al., 2007). According to our source apportionment ~ 81 % - ~ 90 % is of terrestrial origin with 48 ± 19 % of the DOM/DOC stemming from permafrost. The remainder (22 ± 15 %) is most likely aquatic DOM/DOC produced by primary production (fig. 8). The tributaries $\delta^{13}\text{C}$ -signal, showing signs of primary production indicates that these small ice wedge trough streams are not necessarily important for transporting terrestrial OM. Presumably terrestrial OM is rather transported towards the main channel via supra-permafrost base flow, instead of via IWP troughs. Alternatively, terrestrial OM present in the IWP troughs may quickly be decomposed and/or incorporated into primary production. Increased hydrologic connectivity of IWP troughs as well as increased connectivity via active layer deepening in permafrost watersheds (Lafrenière et al., 2019; Evans et al., 2020) may lead to higher input of terrestrial OM.

The exported OC at the outlet is variable in concentration and geochemical signature over time, with three observable patterns: (i) diurnal variation of CDOM abundance and optical properties, (ii) short/storm-induced peaks in POC and dips in DOC and (iii) seasonal decline of DOM export (fig. 3a, b right):

- i. We observed a diurnal pattern in CDOM concentrations (range: ~ 20 % - 25 %) at the stream outlet (fig. 3a right). This diurnal pattern can be explained by both temperature and light dependent variability in productivity as well as variations in ground ice melt contribution and



620 evapotranspiration induced flow effects, which are in turn temperature dependent (Spencer et al.,
2008; Ruhala et al.; 2017). We observe that CDOM fluctuates synchronously with water temperature
(i.e. peaks in water temperature correspond with peaks in CDOM). Similarly, peaks in Sr (~0.9) and
FI (~1.5) correspond with lows in temperature while for HIX this pattern is inverted (fig. S9). This
dynamic may be explained by the increasing importance of primary production with high
temperatures, and decreasing importance of deeper baseflow when temperature decreases (i.e. flow
becomes shallower and the signal less deeply terrestrial). The highest values of HIX are found
around the permafrost table (presumably where baseflow takes place) (fig. S7) and a decrease in
625 HIX at the outlet in sync with lowering temperatures supports the idea of freezing up from below.

ii. A storm event on the 16th and 17th of August resulted in drawdown of CDOM and DOC
concentrations and a sharp spike in POC load (fig. 3a, b right). This shifted the DOC:POC ratio from
an average of 50 to 5.1. We also observed an increase in pH (from ~7 to ~8) and spikes in EC (up
to ~19000 $\mu\text{S cm}^{-1}$ compared to an average of ~900 $\mu\text{S cm}^{-1}$). The storm event was characterized by
630 strong northwesterly winds which, given the shape and orientation of the lagoon are likely to have
pushed water up the stream channel. Due to its proximity to Ptarmigan bay lagoon the autosampler
and multi-parameter probe are likely to have recorded the inflow of lagoon water during storm
springtide. We observed two peaks in POC export with two different terrestrial $\delta^{13}\text{C}$ -POC signals,
the first one (~ -31 ‰ on the 16th) lasted only 6 hours and the second one (~ -27.5 ‰ on the 17th)
635 lingered on for ca. 18 hours before going back to the background signal around -29 ‰. Compared
to the average $\delta^{13}\text{C}$ -POC signal at the outlet, which tends to a more primary produced signal (-29.31
 ± 0.8 ‰ SD. table 3) this jump to -27.5 ‰ seems to be resulting from the input of storm-induced
flushing of terrestrial POC, from overland flow, wind-driven bank erosion, and/or bottom
disturbance in upstream lakes and ponds.

640 iii. Our sensor and sample data show a decreasing trend in both CDOM and DOC concentration during
our sampling period (fig. 3a,b right, fig. S9). This is likely related to a gradual decline in temperature
in the late summer as is illustrated by temperature records from nearby Herschel Island I (fig. S1)
that show our 10-day monitoring period lies on the falling limb of the annual temperature curve. The
decrease in concentrations over time can be caused by (i) a decrease in temperatures and solar
645 irradiation toward the end of summer, leading to lower primary production in the aquatic network.
Additionally, (ii) lower temperatures may decrease the efficiency of OM soil leaching (Whitworth



et al., 2014) over time. And finally, (iii) it may also be likely that the active layer is already starting to freeze-up from below, leading to lower availability of soil DOC. Several studies have looked at seasonal variability of DOC and DOM composition and concluded that antecedent winter DOC is flushed out during freshet, resulting in a DOC peak with relatively low Sr, FI and high SUVA₂₅₄, indicative of DOM coming from the organic surface layer. As the summer season progresses, a steady increase in Sr, and FI and decrease in SUVA₂₅₄ and DOC continuing up to the very end of the season was found uniformly in rivers across the Arctic, linked to the increasing contribution of deeper soil horizons via deepening of the active layer (Neff et al., 2006; Spencer et al., 2008, 2009a; Holmes et al., 2008, 2011). In this respect our study shows similar trends in DOC, SUVA₂₅₄, Sr, and FI at the outlet over the course of the monitoring period.

Our source-apportionment using $\delta^{13}\text{C}$ -DOC, Sr and a₂₅₄/a₃₆₅ as tracers showed that a high proportion of DOC within the stream originates from permafrost DOC contributions (~48 %), outnumbering the DOC influx from the active layer (~31 %) and primary production within the stream (~21 %). This is in stark contrast to larger (Siberian) arctic rivers (Wild et al., 2019), where fluvial DOM fluxes stem predominantly from recent terrestrial primary production sources. Due to the small catchment size the contribution of permafrost OC is likely more evident in small streams and the hiatus between these and larger arctic rivers may indicate that permafrost DOC is likely degraded before it reaches larger rivers. Moreover, small streams like the one in this study drain a degrading continuous permafrost landscape exclusively, whereas large arctic rivers drain also non-permafrost or discontinuous permafrost terrain, disproportionally contributing to the riverine OM fluxes (e.g. Frey and McClelland, 2007). The spatial and temporal extent of terrestrial permafrost inputs into stream networks may likely expand upon increasing severity of meteorological extremes. For instance, Schwab et al. (2020) found aged DOC downstream in the Mackenzie River main stem, following a warm summer and the second warmest winter on record.

This study shows that permafrost-DOM related processes are most visible close to the terrestrial-aquatic interface, i.e. in the headwaters of arctic rivers. With our results we also show that variability herein is highly seasonal and weather driven as our measurements at the outlet show diurnal, storm event and seasonal trend patterns within the duration of our relatively short (10 day) field campaign. This emphasizes the need for high-resolution long-term measurements in order to fully understand the mechanisms at work in the (Arctic) carbon cycles. Important is the



notion that cascading effects and food web interactions resulting from permafrost release into arctic headwaters may be hard to detect, but may have large impacts on sensitive arctic ecosystems (e.g. Vonk et al., 2015a).

4.4 First estimate of regional fluxes from small streams

680 Small coastal tundra watersheds such as Black Creek, presented here, are abundant in and representative for the
lowland regions of the Arctic continuous permafrost zone. Understanding the main controls on OM fluxes and
linkages between soils and streams on the scale presented by us is an important step towards understanding
panarctic carbon and nutrient fluxes. Our results show that small tundra streams have a pronounced terrestrial
DOM signal and a fresher POM signature, but both are highly variable with time and mainly controlled by weather
685 events. The data presented here support the notion that base flow near the permafrost table feeds into small arctic
streams and that during active layer deepening this results in the mobilization of potentially labile organic matter
that has been freeze-locked in permafrost. Transport times through the soil are long (much longer than our 7-day
incubations) and groundwater may be stagnant in some areas, dependent on precipitation or polygon type/drainage
conditions. Hence, our data suggest that a large fraction of (labile) DOM may be utilized before reaching the
690 stream network. Uncertainties concerning the groundwater flow dynamics in permafrost regions make it
extremely difficult to assess biogeochemical responses to hydrological shifts (Lafrenière & Lamoureux, 2019).
The ratio of POC vs DOC in the total OC export, as well as the contributions of in stream production, active layer
and permafrost are variable and our data suggest that this variability is mostly weather and hydrology driven. Due
to their abundance and proximity to the Arctic ocean, small tundra streams have the potential to export large
695 quantities of terrestrial permafrost organic matter into coastal waters. Based on our sampling and measurements
at the outlet (mean discharge of $67 \pm 51.1 \text{ L s}^{-1}$) and mean DOC and POC concentration of $16.0 \pm 3.2 \text{ mg L}^{-1}$ and
 $0.41 \pm 0.2 \text{ mg L}^{-1}$, respectively, together with a delineated catchment area of $\sim 4 \text{ km}^2$, we are able to make first
estimates of seasonal DOC ($\sim 0.03 \pm 0.021 \text{ g DOC m}^{-2} \text{ d}^{-1}$) and POC fluxes ($\sim 0.0006 \pm 0.00065 \text{ g POC m}^{-2} \text{ d}^{-1}$). In
these flux estimates we accounted for the variability in POC concentration due to storms in our sampling period
700 (i.e. the mean POC concentration included the storm days). In contrast to DOC, POC fluxes are likely to be highly
variable since they are impacted by summer storm activity which can vary between 2 and 21 storms per year in
the southern Beaufort Sea region (Hudak & Young, 2002). Arctic-type storms are most prevalent in July and
August and average at 8 storms per season. Assuming a duration of 1-2 days per storm this would lead to an
additional export of $\sim 0.010\text{-}0.020 \text{ g POC m}^{-2}$ annually. The period through which lateral transport of OM occurs
705 is dependent on the thaw season length and the rate at which the seasonal active layer deepens. To estimate



seasonal fluxes, we use an average thaw season duration of 87.7 consecutive frost-free days calculated over the period 1950-2013 from “The Climate Atlas of Canada” (version 2, July 10, 2019, <https://climateatlas.ca>). Using this average, we calculate that Black Creek watershed (~4 km²) exports an average of 8.12 ±6.4 t DOC yr⁻¹ and 0.21 ±0.2 t POC yr⁻¹. We calculated the entire Canadian Yukon Coastal Plain drainage area to be ~17000 km².
710 This yields an approximate 34.51 ±2.7 kt DOC yr⁻¹ and 8.93 ±8.5 kt POC yr⁻¹ for fluvial export. This preliminary scaling assumes that all streams have equally high loads, which is probably an overestimation. For example, larger rivers present in the area are likely to have lower DOC and POC loads as they drain areas with lower OM rich soils and longer transport time and distance allows for more OM processing. With longer, warmer seasons and higher storm frequencies which are predicted for the Arctic (Day et al., 2018), mobilization and export of POC
715 and DOC towards the Arctic Ocean may substantially increase.

4.5 Implications and future research

This study focuses on data retrieved during the latest stage of the thawing season, when active layer depths are at their seasonal maximum. Our results show that OC quality and quantity varies between different soil horizons and landform (i.e. polygon type). Evolution of landforms via degradation of IWP's from LCP to HCP is likely to result
720 in increased drainage and drying of the landscape and increased net runoff as a consequence. Our results show that the balance between lateral and vertical flux is therefore likely to shift toward lateral flux as mobilizable OM will be flushed out of the system more effectively. The shift towards drainage and export rather than within-ecosystem-processing may have strong effects on the arctic lowland tundra biodiversity and food web interactions since these are to a large extent based on wetland-ecosystems (e.g. Vonk et al., 2015a; Liljedahl et al., 2016).

725 In parallel to annual active layer depth deepening, older and potentially more labile OM pools will become available for degradation. In this study we find indications that the most labile fractions are utilized within the soil, and we expect that even in a more well-drained HCP system, residence times within the soil will be long enough to allow for the utilization of the majority of labile DOM. The results show that concentrations of DOC
730 in permafrost are much higher than in the active layer. This together with the notion that labile DOM would be converted quickly leads to the expectation that under current climate trends, small arctic catchments affected by permafrost degradation may export higher loads of recalcitrant DOM. This in turn could impact aquatic food webs in various ways. A recent study by Wologo et al. (2021) suggests that negative priming effects occur as a result of influx of bioavailable permafrost DOM. However, our results show influx of less bioavailable permafrost hence



735 we deem negative priming unlikely. Due to its strong coloration permafrost and deep active layer derived CDOM could significantly impact light dependent processes in the aquatic network. Moreover, chemical composition of permafrost and deep active layer DOM (e.g. high values of ammonium were found) may impact aquatic biogeochemistry. More research is needed to elucidate these ecosystem interactions.

740 To better understand and implement lateral permafrost-OM-dynamics into climate models, more quantitative and qualitative data on the distribution and behavior of small, pan-arctic permafrost catchments is needed. Moreover, there is a simple need to map these watersheds at the basis of the aforementioned challenge. Both, the former and latter could be achieved by more long-term monitoring on a larger spatial scale, e.g. by installing sensors and conducting repetitive field research in designated representative areas as well as by aggregating databases with
745 field and remote sensing data. Lastly, by focusing on optical properties of DOM it is relatively easy and cost-effective to trace changes in watershed biogeochemistry, as optical measurement techniques are uncomplicated and readily available. These techniques together with standardization of methods are there for recommended for a harmonized approach on understanding lateral permafrost-OM-dynamics.

5 Conclusions

750 This study investigates the lateral release of organic matter in an arctic lowland IWP tundra watershed, subject to permafrost degradation. Soil porewater DOM properties and DOC concentrations in the Black Creek catchment vary between thermal layer (i.e. active layer and permafrost) and landform (i.e. LCP and HCP), reflecting differences in drainage patterns and waterlogged conditions. Also, within the active layer, DOM signatures vary between polygon types due to differences in drainage status (i.e. LCP is more water logged, HCP well drained).
755 HCP active layers show a more degraded OM signature. When further arctic warming transitions LCP landscapes into HCP-dominated settings, this may lead to an increasing flux of degraded DOM from soils to streams.

Dissolved carbon yields (mg DOC g^{-1} soil OC) increase with soil depth, yet show a larger variability around the permafrost table. Gleyed soil samples from mineral horizons had relatively high dissolved yields while having
760 low SOC contents, hence accumulation of DOM from other horizons in these gleyed horizons is likely. Porewater incubation experiments show 5-17 % DOC loss after 7 days, with higher losses for active layer than permafrost. The incubated permafrost samples are mostly from within the transition layer where degradation has likely



occurred in the past. Optical properties however indicate increasingly fresh and (potentially) labile OM with depth. Long transport time of porewater DOC within these low-relief catchments suggest that most permafrost DOM is processed/degraded within the soil before it reaches the stream network.

Black Creek transports much more DOC than POC, but storm events change that ratio by an order of magnitude. Our 10-day monitoring period shows diurnal, weather-driven, and long-term patterns in OC concentrations and properties. Source apportionment of stream DOC using $\delta^{13}\text{C}$ and DOM-spectral signatures show a dominance of terrestrial OC over autochthonous production, and a deep active layer/permafrost-DOC contribution around 48 %. This contrasts with larger arctic fluvial systems that are dominated by recent terrestrial production. First upscaling estimates of annual Black Creek fluxes give values of $8.12 \pm 6.4 \text{ t DOC yr}^{-1}$ and $0.21 \pm 0.2 \text{ t POC yr}^{-1}$. Rough upscaling to the entire Canadian Yukon Coastal Plain drainage area ($\sim 17000 \text{ km}^2$) yields an approximate $34.51 \pm 2.7 \text{ kt DOC yr}^{-1}$ and $8.93 \pm 8.5 \text{ kt POC yr}^{-1}$ by fluvial export.

High frequency measurements at the outlet in combination with in-situ weather observations underline the highly variable nature of small arctic watersheds and their susceptibility to changes. To get a more thorough understanding of arctic watersheds and their responses to climate change and permafrost degradation, it is important that more geographically widespread and longer timespan covering monitoring efforts of these streams are implemented, e.g. through sensor installations, use of cost-effective optical proxies to monitor change. Further, combining remote sensing data with field observations and machine learning techniques pose a powerful tool for upscaling.

Acknowledgements

We thank all those who have made contributions that have led to this publication. We thank the Yukon Territorial Government, Yukon Parks (Herschel Island Qikiqtaryuk Territorial Park), and the Aurora Research Institute for their support during this project. The work presented here was done under the Nunataryuk project, which received funding under the European Union's Horizon 2020 Research and Innovation Program under Grant Agreement 773421. We wish to express our special gratitude to C. Stedmon for providing laboratory access, equipment and guidance. And to S. Verdegaal-Warmerdam, A. Dalhoff Bruhn Jensen, C. Burau, J. Gimsa, S. Stettner, A. Beamish, K. Klein, R. Broekman, R. van Logtestijn, M. Sanchez Roman, M. Fritz and L. Bröder for laboratory



analysis, and field and laboratory assistance and conceptualization of the research project. We thank S. McLeod, P. Archie and F. Dillon for their helpful insights and support in the field.



References

- AMAP: Snow, Water, Ice and Permafrost in the Arctic, 2017.
- 800 Coch, C., Lamoureux, S. F., Knoblauch, C., Eiseheid, I., Fritz, M., Obu, J., and Lantuit, H.: Summer rainfall dissolved organic carbon, solute, and sediment fluxes in a small Arctic coastal catchment on Herschel Island (Yukon Territory, Canada), *Arct. Sci.*, <https://doi.org/10.1139/as-2018-0010>, 2018.
- Cory, R. M., Miller, M. P., Mcknight, D. M., Guerard, J. J., and Miller, P. L.: Effect of instrument-specific response on the analysis of fulvic acid fluorescence spectra, *Limnol. Oceanogr. Methods*, 8, <https://doi.org/10.4319/lom.2010.8.67>, 2010.
- 805 Fouché, J., Christiansen, C. T., Lafrenière, M. J., Grogan, P., and Lamoureux, S. F.: Canadian permafrost stores large pools of ammonium and optically distinct dissolved organic matter, *Nat. Commun.*, 11, <https://doi.org/10.1038/s41467-020-18331-w>, 2020.
- Holmes, R. M., McClelland, J. W., Peterson, B. J., Tank, S. E., Bulygina, E., Eglinton, T. I., Gordeev, V. V., Gurtovaya, T. Y., Raymond, P. A., Repeta, D. J., Staples, R., Striegl, R. G., Zhulidov, A. V., and Zimov, S. A.: Seasonal and Annual Fluxes of Nutrients and Organic Matter from Large Rivers to the Arctic Ocean and Surrounding Seas, *Estuaries Coasts*, <https://doi.org/10.1007/s12237-011-9386-6>, 2012.
- 810 Hudak, D. R. and Young, J. M. C.: Storm climatology of the Southern Beaufort sea, *Atmosphere - Ocean*, <https://doi.org/10.3137/ao.400205>, 2002.
- Hugelius, G., Strauss, J. (orcid:0000000346784982), Zubrzycki, S. (orcid:0000000263989173), Harden, J. W., Schuur, E. a G., Ping, C.-L., Schirmer, L., Grosse, G., Michaelson, G. J., Koven, C. D., O'Donnell, J. A., Elberling, B., Mishra, U., Camill, P., Yu, Z., Palmtag, J., and Kuhry, P.: Estimated stocks of circumpolar permafrost carbon with quantified uncertainty ranges and identified data gaps, *Biogeosciences Online*, 11, <https://doi.org/10.5194/bg-11-6573-2014>, 2014.
- van Huissteden, J. and Dolman, A. J.: Soil carbon in the Arctic and the permafrost carbon feedback, *Curr. Opin. Environ. Sustain.*, 4, 545–551, <https://doi.org/10.1016/j.cosust.2012.09.008>, 2012.
- 820 Jones, E., Oliphant, T., Peterson, P., and Others: SciPy: Open Source Scientific Tools for Python, 2001 (<http://www.scipy.org/>), 2015.
- Kaiser, K., Guggenberger, G., and Zech, W.: Isotopic fractionation of dissolved organic carbon in shallow forest soils as affected by sorption, *Eur. J. Soil Sci.*, <https://doi.org/10.1046/j.1365-2389.2001.00407.x>, 2001.
- 825 Kawahigashi, M., Kaiser, K., Kalbitz, K., Rodionov, A., and Guggenberger, G.: Dissolved organic matter in small streams along a gradient from discontinuous to continuous permafrost, *Glob. Change Biol.*, 10, 1576–1586, <https://doi.org/10.1111/j.1365-2486.2004.00827.x>, 2004.



- Knoblauch, C., Beer, C., Sosnin, A., Wagner, D., and Pfeiffer, E. M.: Predicting long-term carbon mineralization and trace gas production from thawing permafrost of Northeast Siberia, *Glob. Change Biol.*, 19, <https://doi.org/10.1111/gcb.12116>, 2013.
- 830 Koven, C. D., Ringeval, B., Friedlingstein, P., Ciais, P., Cadule, P., Khvorostyanov, D., Krinner, G., and Tarnocai, C.: Permafrost carbon-climate feedbacks accelerate global warming, *Proc. Natl. Acad. Sci. U. S. A.*, <https://doi.org/10.1073/pnas.1103910108>, 2011.
- Lafrenière, M. J. and Lamoureux, S. F.: Effects of changing permafrost conditions on hydrological processes and fluvial fluxes, 2019.
- 835 Lee, H., Schuur, E. A. G., Inglett, K. S., Lavoie, M., and Chanton, J. P.: The rate of permafrost carbon release under aerobic and anaerobic conditions and its potential effects on climate, *Glob. Change Biol.*, 18, <https://doi.org/10.1111/j.1365-2486.2011.02519.x>, 2012.
- Lee, M. H., Lee, S. Y., Yoo, H. Y., Shin, K. H., and Hur, J.: Comparing optical versus chromatographic descriptors of dissolved organic matter (DOM) for tracking the non-point sources in rural watersheds, *Ecol. Indic.*, 117, <https://doi.org/10.1016/j.ecolind.2020.106682>, 2020.
- 840 Lewis, T. and Lamoureux, S. F.: Twenty-first century discharge and sediment yield predictions in a small high Arctic watershed, *Glob. Planet. Change*, 71, <https://doi.org/10.1016/j.gloplacha.2009.12.006>, 2010.
- Lewis, T., Lafrenière, M. J., and Lamoureux, S. F.: Hydrochemical and sedimentary responses of paired High Arctic watersheds to unusual climate and permafrost disturbance, Cape Bounty, Melville Island, Canada, *Hydrol. Process.*, <https://doi.org/10.1002/hyp.8335>, 2012.
- 845 Liljedahl, A., Hinzman, L. D., and Schulla, J.: Ice-wedge polygon type controls low-gradient watershed-scale hydrology, 2012.
- Liljedahl, A. K., Boike, J., Daanen, R. P., Fedorov, A. N., Frost, G. V., Grosse, G., Hinzman, L. D., Iijma, Y., Jorgenson, J. C., Matveyeva, N., Necsoiu, M., Reynolds, M. K., Romanovsky, V. E., Schulla, J., Tape, K. D., Walker, D. A., Wilson, C. J., Yabuki, H., and Zona, D.: Pan-Arctic ice-wedge degradation in warming permafrost and its influence on tundra hydrology, *Nat. Geosci.*, <https://doi.org/10.1038/ngeo2674>, 2016.
- 850 MacDonald, E. N., Tank, S. E., Kokelj, S. V., Froese, D. G., and Hutchins, R. H. S.: Permafrost-derived dissolved organic matter composition varies across permafrost end-members in the western Canadian Arctic, *Environ. Res. Lett.*, 16, <https://doi.org/10.1088/1748-9326/abd971>, 2021.
- 855 MacDougall, A. H., Avis, C. A., and Weaver, A. J.: Significant contribution to climate warming from the permafrost carbon feedback, *Nat. Geosci.*, <https://doi.org/10.1038/ngeo1573>, 2012.
- Mackay, J. R.: The World Of Underground Ice, *Ann. Assoc. Am. Geogr.*, 62, <https://doi.org/10.1111/j.1467-8306.1972.tb00839.x>, 1972.



- 860 Mann, P. J., Davydova, A., Zimov, N., Spencer, R. G. M., Davydov, S., Bulygina, E., Zimov, S., and Holmes, R. M.: Controls on the composition and lability of dissolved organic matter in Siberia's Kolyma River basin, *J. Geophys. Res. Biogeosciences*, 117, <https://doi.org/10.1029/2011JG001798>, 2012.
- Mann, P. J., Eglinton, T. I., McIntyre, C. P., Zimov, N., Davydova, A., Vonk, J. E., Holmes, R. M., and Spencer, R. G. M.: Utilization of ancient permafrost carbon in headwaters of Arctic fluvial networks, *Nat. Commun.*, 6, 7856, <https://doi.org/10.1038/ncomms8856>, 2015.
- 865 Mcguire, A. D., Anderson, L. G., Christensen, T. R., Scott, D., Laodong, G., Hayes, D. J., Martin, H., Lorenson, T. D., Macdonald, R. W., and Nigal, R.: Sensitivity of the carbon cycle in the Arctic to climate change, 2009.
- McKinney, W.: Data Structures for Statistical Computing in Python, Proceedings of the 9th Python in Science Conference, <https://doi.org/10.25080/majora-92bf1922-00a>, 2010.
- 870 McKnight, D. M., Boyer, E. W., Westerhoff, P. K., Doran, P. T., Kulbe, T., and Andersen, D. T.: Spectrofluorometric characterization of dissolved organic matter for indication of precursor organic material and aromaticity, *Limnol. Oceanogr.*, 46, 38–48, <https://doi.org/10.4319/lo.2001.46.1.0038>, 2001.
- Meredith, M.: SPM 203 3 Polar Regions Coordinating Lead Authors, n.d.
- Morin, P., Porter, C., Cloutier, M., Howat, I., Noh, M.-J., Willis, M., Bates, B., Williamson, C., and Peterman, K.: ArcticDEM; A Publically Available, High Resolution Elevation Model of the Arctic, *Geophys. Res. Abstr.*, 18, 2016.
- 875 Murphy, K. R., Stedmon, C. A., Graeber, D., and Bro, R.: Fluorescence spectroscopy and multi-way techniques. PARAFAC, *Anal. Methods*, 5, 6557–6566, <https://doi.org/10.1039/C3AY41160E>, 2013.
- Natali, S. M., Schuur, E. A. G., Webb, E. E., Pries, C. E. H., and Crummer, K. G.: Permafrost degradation stimulates carbon loss from experimentally warmed tundra, *Ecology*, 95, <https://doi.org/10.1890/13-0602.1>, 2014.
- 880 Neff, J. C., Finlay, J. C., Zimov, S. A., Davydov, S. P., Carrasco, J. J., Schuur, E. a G., and Davydova, A. I.: Seasonal changes in the age and structure of dissolved organic carbon in Siberian rivers and streams, *Geophys. Res. Lett.*, 33, <https://doi.org/10.1029/2006GL028222>, 2006.
- 885 Obu, J., Westermann, S., Bartsch, A., Berdnikov, N., Christiansen, H. H., Dashtseren, A., Delaloye, R., Elberling, B., Etzelmüller, B., Kholodov, A., Khomutov, A., Kääh, A., Leibman, M. O., Lewkowicz, A. G., Panda, S. K., Romanovsky, V., Way, R. G., Westergaard-Nielsen, A., Wu, T., Yamkhin, J., and Zou, D.: Northern Hemisphere permafrost map based on TTOP modelling for 2000–2016 at 1 km² scale, 2019.
- Ohno, T.: Fluorescence inner-filtering correction for determining the humification index of dissolved organic matter, *Environ. Sci. Technol.*, <https://doi.org/10.1021/es0155276>, 2002.



- 890 Olefeldt, D., Goswami, S., Grosse, G., Hayes, D., Hugelius, G., Kuhry, P., McGuire, A. D., Romanovsky, V. E., Sannel, A. B. K., Schuur, E. A. G., and Turetsky, M. R.: Circumpolar distribution and carbon storage of thermokarst landscapes, *Nat. Commun.*, <https://doi.org/10.1038/ncomms13043>, 2016.
- Parlanti, E., Wörz, K., Geoffroy, L., and Lamotte, M.: Dissolved organic matter fluorescence spectroscopy as a tool to estimate biological activity in a coastal zone submitted to anthropogenic inputs, *Org. Geochem.*, 31, 1765–1781, [https://doi.org/10.1016/S0146-6380\(00\)00124-8](https://doi.org/10.1016/S0146-6380(00)00124-8), 2000.
- 895 Parmentier, F. J. W., Christensen, T. R., Rysgaard, S., Bendtsen, J., Glud, R. N., Else, B., van Huissteden, J., Sachs, T., Vonk, J. E., and Sejr, M. K.: A synthesis of the arctic terrestrial and marine carbon cycles under pressure from a dwindling cryosphere, *Ambio*, <https://doi.org/10.1007/s13280-016-0872-8>, 2017.
- 900 Plaza, C., Pegoraro, E., Bracho, R., Celis, G., Crummer, K. G., Hutchings, J. A., Hicks Pries, C. E., Mauritz, M., Natali, S. M., Salmon, V. G., Schädel, C., Webb, E. E., and Schuur, E. A. G.: Direct observation of permafrost degradation and rapid soil carbon loss in tundra, *Nat. Geosci.*, 12, <https://doi.org/10.1038/s41561-019-0387-6>, 2019.
- Prowse, T. D. and Flegg, P. O.: Arctic River Flow: A Review of Contributing Areas, in: *The Freshwater Budget of the Arctic Ocean*, 2000.
- Rampton, V. N.: Quaternary Geology of the Yukon Coastal Plain, *Geol. Surv. Can. Bull.* 317, 1982.
- 905 van Rossum, G. and Drake, F. L.: *Python 3 Reference Manual.*, 2009.
- Ruhala, S. S. and Zarnetske, J. P.: Using in-situ optical sensors to study dissolved organic carbon dynamics of streams and watersheds: A review, 2017.
- Schoeneberger, P. J., Wysocki, D. A., Benham, E. C., and Soil Survey Staff: *Field Book for Describing and Sampling Soils, Version 3.0.* Natural Resources Conservation Service. National Soil Survey Center, Lincoln, NE., 2012.
- 910 Schuur, E. A. G., Vogel, J. G., Crummer, K. G., Lee, H., Sickman, J. O., and Osterkamp, T. E.: The effect of permafrost thaw on old carbon release and net carbon exchange from tundra, *Nature*, 459, <https://doi.org/10.1038/nature08031>, 2009.
- 915 Schuur, E. a G., McGuire, A. D., Schädel, C., Grosse, G., Harden, J. W., Hayes, D. J., Hugelius, G., Koven, C. D., Kuhry, P., Lawrence, D. M., Natali, S. M., Olefeldt, D., Romanovsky, V. E., Schaefer, K., Turetsky, M. R., Treat, C. C., and Vonk, J. E.: Climate change and the permafrost carbon feedback, *Nature*, 520, 171–179, <https://doi.org/10.1038/nature14338>, 2015.
- 920 Schwab, M. S., Hilton, R. G., Raymond, P. A., Haghipour, N., Amos, E., Tank, S. E., Holmes, R. M., Tipper, E. T., and Eglinton, T. I.: An Abrupt Aging of Dissolved Organic Carbon in Large Arctic Rivers, *Geophys. Res. Lett.*, 47, <https://doi.org/10.1029/2020GL088823>, 2020.



- Screen, J. A., Deser, C., and Simmonds, I.: Local and remote controls on observed Arctic warming, *Geophys. Res. Lett.*, 39, <https://doi.org/10.1029/2012GL051598>, 2012.
- Seabold, S. and Perktold, J.: Statsmodels: Econometric and Statistical Modeling with Python, Proceedings of the 9th Python in Science Conference, <https://doi.org/10.25080/majora-92bf1922-011>, 2010.
- 925 Selvam, B. P., Lapierre, J. F., Guillemette, F., Voigt, C., Lamprecht, R. E., Biasi, C., Christensen, T. R., Martikainen, P. J., and Berggren, M.: Degradation potentials of dissolved organic carbon (DOC) from thawed permafrost peat, *Sci. Rep.*, 7, 45811, <https://doi.org/10.1038/srep45811>, 2017.
- Shatilla, N. and Carey, S.: Assessing inter-annual and seasonal patterns of DOC and DOM quality across a complex alpine watershed underlain by discontinuous permafrost in Yukon, Canada, *Hydrol. Earth Syst. Sci.*, 930 <https://doi.org/10.5194/hess-23-3571-2019>, 2019.
- Shirokova, L. S., Chupakov, A., Zabelina, S., Neverova, N., Payandi-Rolland, D., Causserand, C., Karlsson, J., and Pokrovsky, O. S.: Humic surface waters of frozen peat bogs (permafrost zone) are highly resistant to bio- and photodegradation, *Biogeosciences*, <https://doi.org/10.5194/bg-16-2511-2019>, 2019.
- 935 Spencer, R. G. M., Aiken, G. R., Wickland, K. P., Striegl, R. G., and Hernes, P. J.: Seasonal and spatial variability in dissolved organic matter quantity and composition from the Yukon River basin, Alaska, *Glob. Biogeochem. Cycles*, 22, <https://doi.org/10.1029/2008GB003231>, 2008.
- Spencer, R. G. M., Aiken, G. R., Butler, K. D., Dornblaser, M. M., Striegl, R. G., and Hernes, P. J.: Utilizing chromophoric dissolved organic matter measurements to derive export and reactivity of dissolved organic carbon exported to the Arctic Ocean: A case study of the Yukon River, Alaska, *Geophys. Res. Lett.*, 36, 940 <https://doi.org/10.1029/2008GL036831>, 2009.
- Spencer, R. G. M., Mann, P. J., Dittmar, T., Eglinton, T. I., McIntyre, C., Holmes, R. M., Zimov, N., and Stubbins, A.: Detecting the signature of permafrost thaw in Arctic rivers, *Geophys. Res. Lett.*, 42, 2015GL063498, <https://doi.org/10.1002/2015GL063498>, 2015.
- 945 Stedmon, C. A. and Nelson, N. B.: The Optical Properties of DOM in the Ocean, in: *Biogeochemistry of Marine Dissolved Organic Matter: Second Edition*, 2015.
- Tank, S. E., Lesack, L. F. W., Gareis, J. A. L., Osburn, C. L., and Hesslein, R. H.: Multiple tracers demonstrate distinct sources of dissolved organic matter to lakes of the Mackenzie Delta, Western Canadian Arctic, *Limnol. Oceanogr.*, 56, <https://doi.org/10.4319/lo.2011.56.4.1297>, 2011.
- 950 Tank, S. E., Vonk, J. E., Walvoord, M. A., McClelland, J. W., Laurion, I., and Abbott, B. W.: Landscape matters: Predicting the biogeochemical effects of permafrost thaw on aquatic networks with a state factor approach, *Permafrost and Periglacial Processes*, <https://doi.org/10.1002/ppp.2057>, 2020.
- Teufel, B. and Sushama, L.: Abrupt changes across the Arctic permafrost region endanger northern development, 2019.



- 955 Throckmorton, H. M., Newman, B. D., Heikoop, J. M., Perkins, G. B., Feng, X., Graham, D. E., O'Malley, D., Vesselinov, V. V., Young, J., Wullschleger, S. D., and Wilson, C. J.: Active layer hydrology in an arctic tundra ecosystem: quantifying water sources and cycling using water stable isotopes, *Hydrol. Process.*, <https://doi.org/10.1002/hyp.10883>, 2016.
- 960 Vonk, J. E., Sanchez-Garca, L., Van Dongen, B. E., Alling, V., Kosmach, D., Charkin, A., Semiletov, I. P., Dudarev, O. V., Shakhova, N., Roos, P., Eglinton, T. I., Andersson, A., and Gustafsson, A.: Activation of old carbon by erosion of coastal and subsea permafrost in Arctic Siberia, *Nature*, 489, <https://doi.org/10.1038/nature11392>, 2012.
- Vonk, J. E., Mann, P. J., Dowdy, K. L., Davydova, A., Davydov, S. P., Zimov, N., Spencer, R. G. M., Bulygina, E. B., Eglinton, T. I., and Holmes, R. M.: Dissolved organic carbon loss from Yedoma permafrost amplified by ice wedge thaw, *Environ. Res. Lett.*, 8, 35023, <https://doi.org/10.1088/1748-9326/8/3/035023>, 2013.
- 965 Vonk, J. E., Semiletov, I. P., Dudarev, O. V., Eglinton, T. I., Andersson, A., Shakhova, N., Charkin, A., Heim, B., and Gustafsson, Ö.: Preferential burial of permafrost-derived organic carbon in Siberian-Arctic shelf waters, *J. Geophys. Res. Oceans*, 119, <https://doi.org/10.1002/2014JC010261>, 2014.
- 970 Vonk, J. E., Tank, S. E., Mann, P. J., Spencer, R. G. M., Treat, C. C., Striegl, R. G., Abbott, B. W., and Wickland, K. P.: Biodegradability of dissolved organic carbon in permafrost soils and aquatic systems: A meta-analysis, *Biogeosciences*, 12, <https://doi.org/10.5194/bg-12-6915-2015>, 2015a.
- Vonk, J. E., Tank, S. E., Bowden, W. B., Laurion, I., Vincent, W. F., Alekseychik, P., Amyot, M., Billet, M. F., Canário, J., Cory, R. M., Deshpande, B. N., Helbig, M., Jammert, M., Karlsson, J., Larouche, J., Macmillan, G., Rautio, M., Walter Anthony, K. M., and Wickland, K. P.: Reviews and syntheses: Effects of permafrost thaw on Arctic aquatic ecosystems, 2015b.
- 975 Vonk, J. E., Tank, S. E., Bowden, W. B., Laurion, I., Vincent, W. F., Alekseychik, P., Amyot, M., Billet, M. F., Canário, J., Cory, R. M., Deshpande, B. N., Helbig, M., Jammert, M., Karlsson, J., Larouche, J., Macmillan, G., Rautio, M., Walter Anthony, K. M., and Wickland, K. P.: Reviews and syntheses: Effects of permafrost thaw on Arctic aquatic ecosystems, 2015c.
- 980 Vonk, J. E., Tank, S. E., and Walvoord, M. A.: Integrating hydrology and biogeochemistry across frozen landscapes, 2019.
- Wainwright, H. M., Dafflon, B., Smith, L. J., Hahn, M. S., Curtis, J. B., Wu, Y., Ulrich, C., Peterson, J. E., Torn, M. S., and Hubbard, S. S.: Identifying multiscale zonation and assessing the relative importance of polygon geomorphology on carbon fluxes in an Arctic tundra ecosystem, *J. Geophys. Res. Biogeosciences*, 120, <https://doi.org/10.1002/2014JG002799>, 2015.
- 985 Wales, N. A., Gomez-Velez, J. D., Newman, B. D., Wilson, C. J., Dafflon, B., Kneafsey, T. J., Soom, F., and Wullschleger, S. D.: Understanding the relative importance of vertical and horizontal flow in ice-wedge polygons, *Hydrol. Earth Syst. Sci.*, <https://doi.org/10.5194/hess-24-1109-2020>, 2020.



- Walker, D. A., Daniëls, F. J. A., Matveyeva, N. V., Šibík, J., Walker, M. D., Breen, A. L., Druckenmiller, L. A., Reynolds, M. K., Bültmann, H., Hennekens, S., Buchhorn, M., Epstein, H. E., Ermokhina, K., Fosaa, A. M., Heidmarsson, S., Heim, B., Jónsdóttir, I. S., Koroleva, N., Lévesque, E., MacKenzie, W. H., Henry, G. H. R., Nilsen, L., Peet, R., Razzhivin, V., Talbot, S. S., Telyatnikov, M., Thannheiser, D., Webber, P. J., and Wirth, L. M.: Circumpolar Arctic Vegetation Classification, *Phytocoenologia*, 48, <https://doi.org/10.1127/phyto/2017/0192>, 2018.
- 990
- Walvoord, M. A. and Kurylyk, B. L.: Hydrologic Impacts of Thawing Permafrost-A Review, *Vadose Zone J.*, <https://doi.org/10.2136/vzj2016.01.0010>, 2016.
- 995
- Wauthy, M., Rautio, M., Christoffersen, K. S., Forsström, L., Laurion, I., Mariash, H. L., Peura, S., and Vincent, W. F.: Increasing dominance of terrigenous organic matter in circumpolar freshwaters due to permafrost thaw, *Limnol. Oceanogr. Lett.*, 3, 186–198, <https://doi.org/10.1002/lo12.10063>, 2018.
- Weishaar, J. L., Aiken, G. R., Bergamaschi, B. A., Fram, M. S., Fujii, R., and Mopper, K.: Evaluation of specific ultraviolet absorbance as an indicator of the chemical composition and reactivity of dissolved organic carbon, *Environ. Sci. Technol.*, <https://doi.org/10.1021/es030360x>, 2003.
- 1000
- Whitworth, K. L., Baldwin, D. S., and Kerr, J. L.: The effect of temperature on leaching and subsequent decomposition of dissolved carbon from inundated floodplain litter: Implications for the generation of hypoxic blackwater in lowland floodplain rivers, *Chem. Ecol.*, 30, <https://doi.org/10.1080/02757540.2014.885019>, 2014.
- 1005
- Wild, B., Andersson, A., Bröder, L., Vonk, J., Hugelius, G., McClelland, J. W., Song, W., Raymond, P. A., and Gustafsson, Ö.: Rivers across the Siberian Arctic unearth the patterns of carbon release from thawing permafrost, *Proc. Natl. Acad. Sci. U. S. A.*, <https://doi.org/10.1073/pnas.1811797116>, 2019.
- Wilson, H. F. and Xenopoulos, M. A.: Effects of agricultural land use on the composition of fluvial dissolved organic matter, *Nat. Geosci.*, 2, <https://doi.org/10.1038/ngeo391>, 2009.
- 1010
- Wologo, E., Shakil, S., Zolkos, S., Textor, S., Ewing, S., Klassen, J., Spencer, R. G. M., Podgorski, D. C., Tank, S. E., Baker, M. A., O'Donnell, J. A., Wickland, K. P., Foks, S. S. W., Zarnetske, J. P., Lee-Cullin, J., Liu, F., Yang, Y., Kortelainen, P., Kolehmainen, J., Dean, J. F., Vonk, J. E., Holmes, R. M., Pinay, G., Powell, M. M., Howe, J., Frei, R. J., Bratsman, S. P., and Abbott, B. W.: Stream Dissolved Organic Matter in Permafrost Regions Shows Surprising Compositional Similarities but Negative Priming and Nutrient Effects, *Glob. Biogeochem. Cycles*, 35, <https://doi.org/10.1029/2020GB006719>, 2021.
- 1015
- Wooller, M. J., Zazula, G. D., Edwards, M., Froese, D. G., Boone, R. D., Parker, C., and Bennett, B.: Stable carbon isotope compositions of Eastern Beringian grasses and sedges: Investigating their potential as paleoenvironmental indicators, *Arct. Antarct. Alp. Res.*, 39, [https://doi.org/10.1657/1523-0430\(2007\)39\[318:SCICOE\]2.0.CO;2](https://doi.org/10.1657/1523-0430(2007)39[318:SCICOE]2.0.CO;2), 2007.
- 1020
- Zhang, T., Barry, R. G., Knowles, K., Heginbottom, J. A., and Brown, J.: Statistics and characteristics of permafrost and ground-ice distribution in the Northern Hemisphere, *Polar Geogr.*, 23, <https://doi.org/10.1080/10889379909377670>, 1999.



Zimov, S. A.: CLIMATE CHANGE: Permafrost and the Global Carbon Budget, *Science*, 312, 1612–1613, <https://doi.org/10.1126/science.1128908>, 2006.

1025

FIGURE 1. SITUATION OF BLACK CREEK WATERSHED ON THE YUKON COASTAL PLAIN 38

1030 FIGURE 2. EXAMPLE OF ICE WEDGE POLYGON TYPES 39

FIGURE 3. STREAM DOC AND $\delta^{13}\text{C}$ -DOC TIMESERIES AT THE OUTLET AND UPSTREAM 40

FIGURE 4. POREWATER DOC CONCENTRATION AND YIELD VS ACTIVE LAYER DEPTH 41

1035

FIGURE 5. LOSS OF DOC (%) AND $\delta^{13}\text{C}$ -DOC AFTER 7 DAYS INCUBATION 42

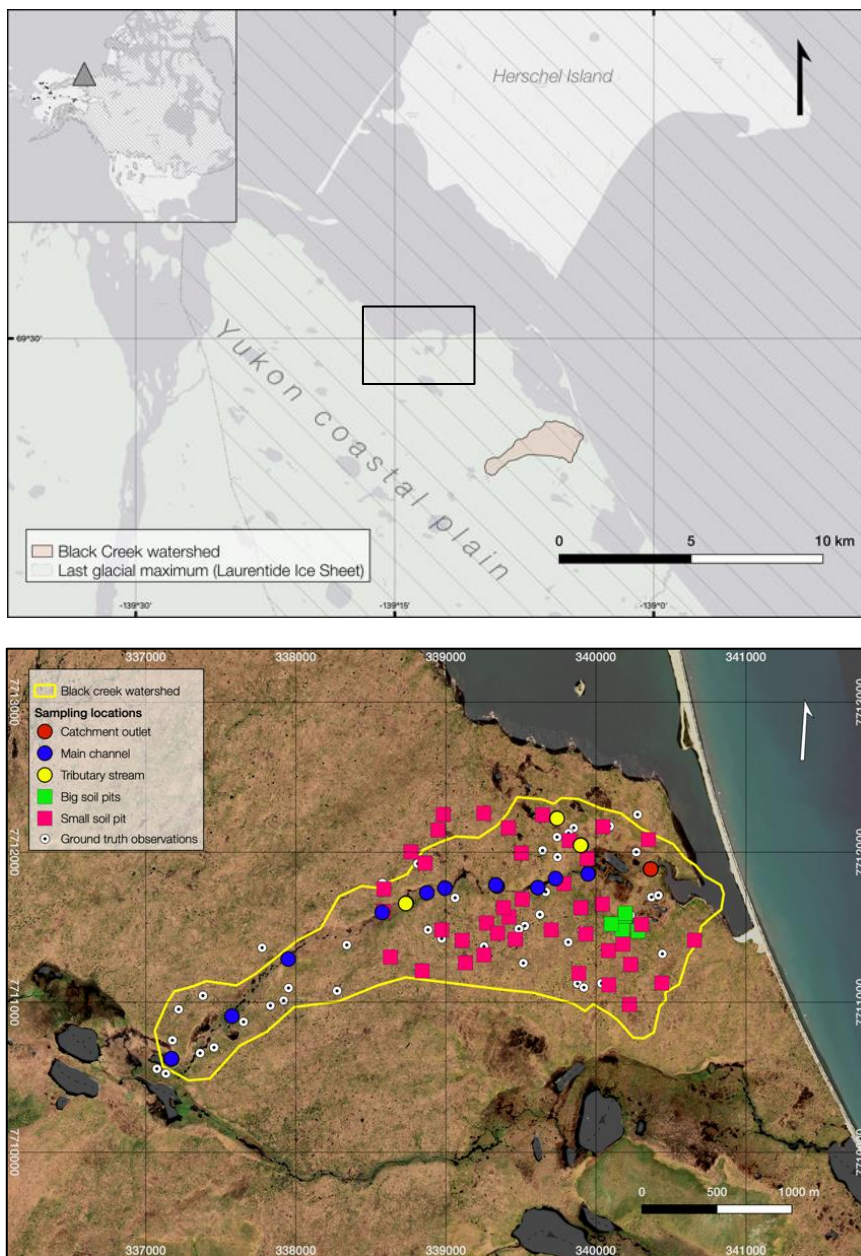
FIGURE 6. SUVA₂₅₄, SLOPE RATIO (SR) AND HUMIFICATION INDEX (HIX) IN POREWATERS 43

1040 FIGURE 7. DOC CONCENTRATION AND SOC CONTENT VS DEPTH TO THE PERMAFROST 44

FIGURE 8. MODELED DOM SOURCE CONTRIBUTIONS 45



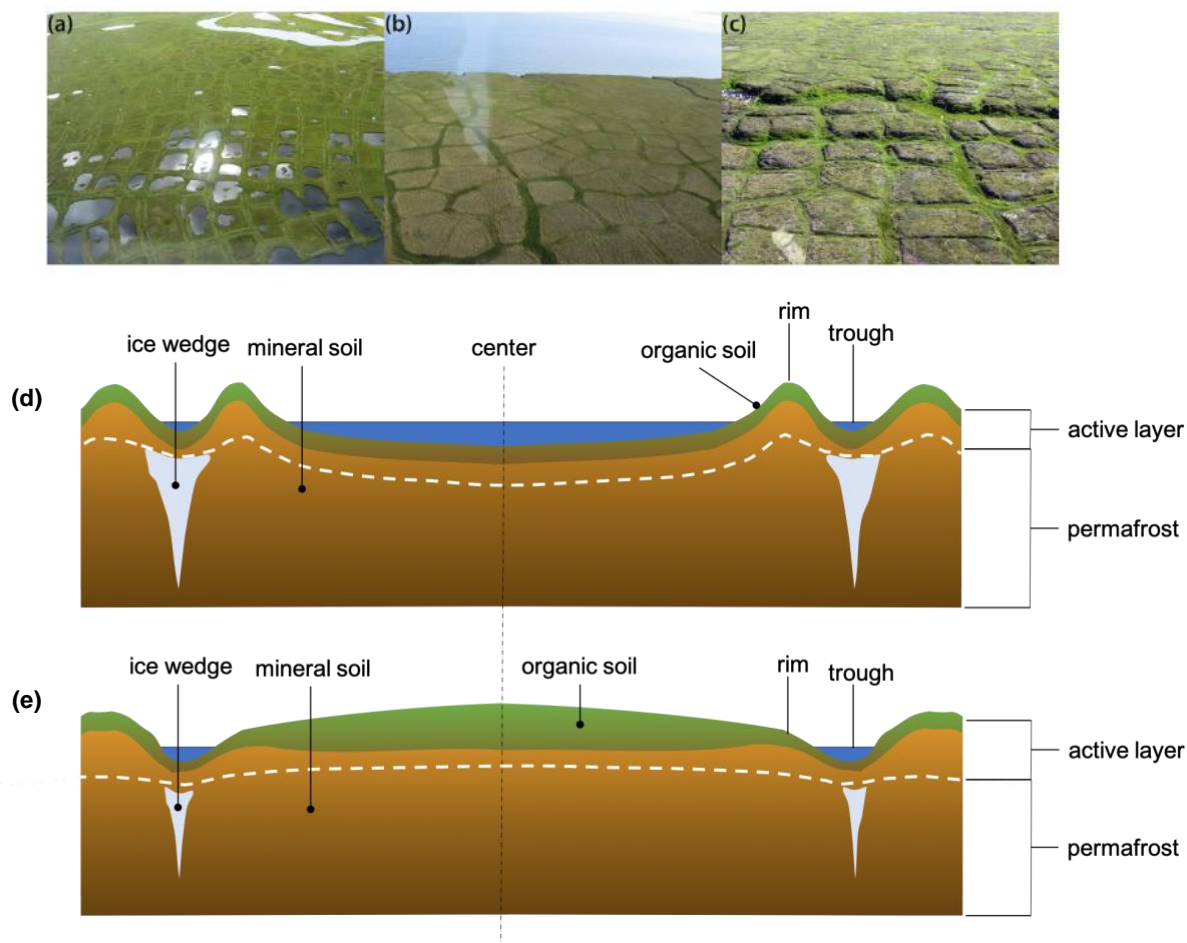
Main Figures



1045 **Figure 1.** Location of Black Creek watershed on the Yukon coastal plain (upper panel) and detailed catchment image showing the different sampling locations and sampling types (lower panel) (satellite imagery: WorldView-2, DigitalGlobe Inc., acquired on July 18, 2018).



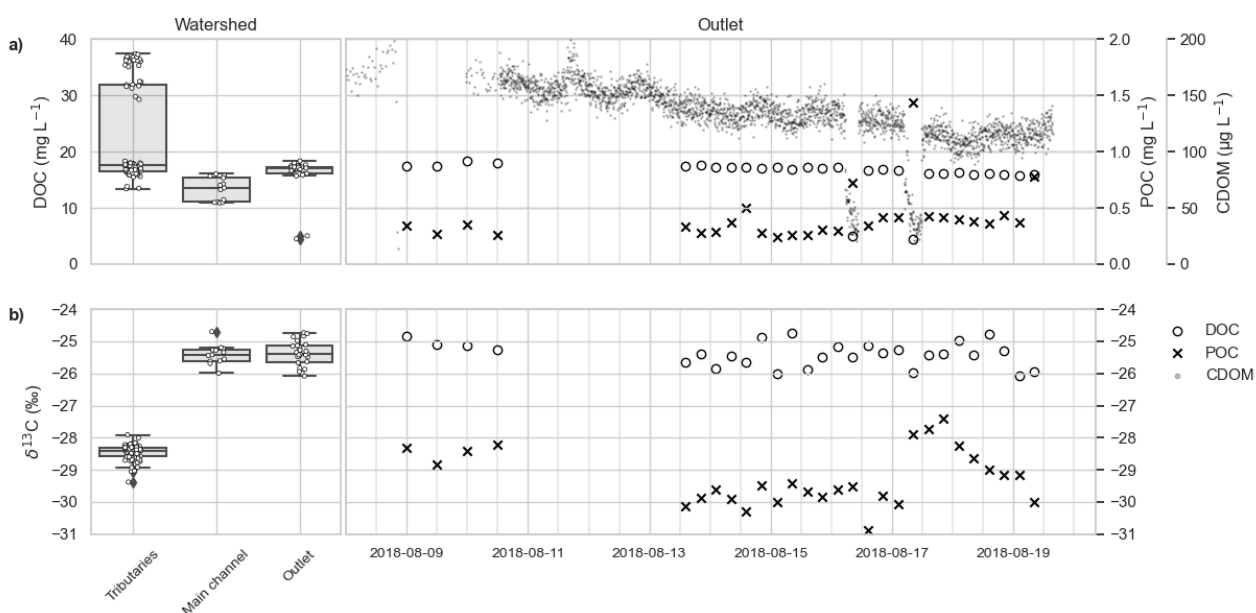
Main Figures



1050 **Figure 2.** Examples of typical low (a), flat (b) and high (c) centered polygons as seen along the Yukon coast (adapted from Fritz et al., 2016). Schematic of a low centered polygon (d) and high centered polygon (e).



Main Figures



1055 **Figure 3.** DOC concentrations (mg/L) measured within tributaries, main channel and outlet (panel A, left),
and POC (mg/L; crosses), DOC (mg/L; circles; note scale is on left panel) and cDOM (μg/L; filled small
1060 circles) concentrations within stream water at the watershed outlet over time (panel A, right). δ¹³C-DOC
isotopic signal within tributaries, main channel and outlet (panel B, left), and δ¹³C-DOC and δ¹³C-POC over
time at the catchment outlet (panel B, right). Note that two clear drops in the CDOM measurements on the
16th and 17th of August mark a storm event. This is also visible in the δ¹³C-POC and to lesser extent δ¹³C-
DOC source shift (B, right) around these dates.

1065



Main Figures

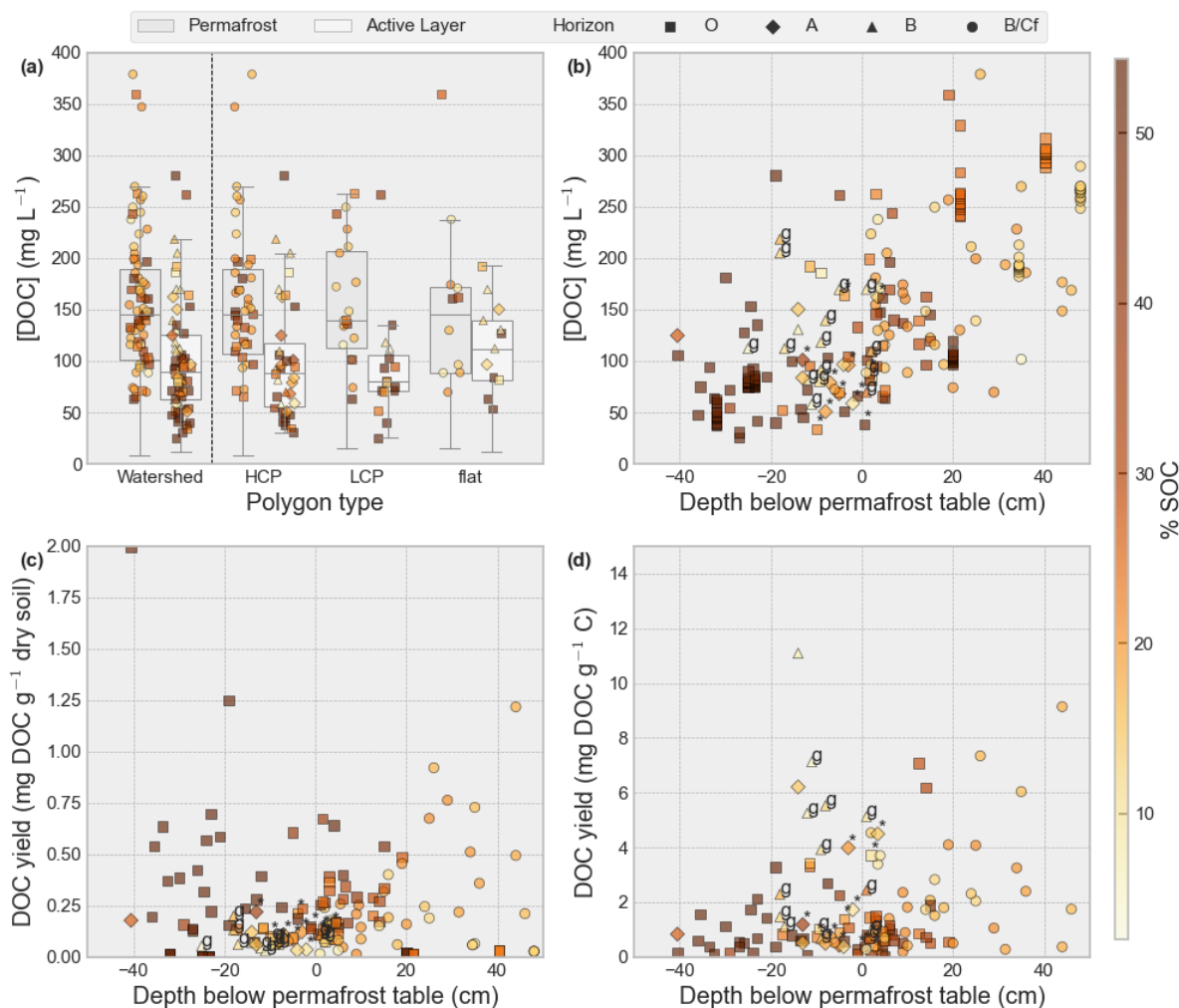
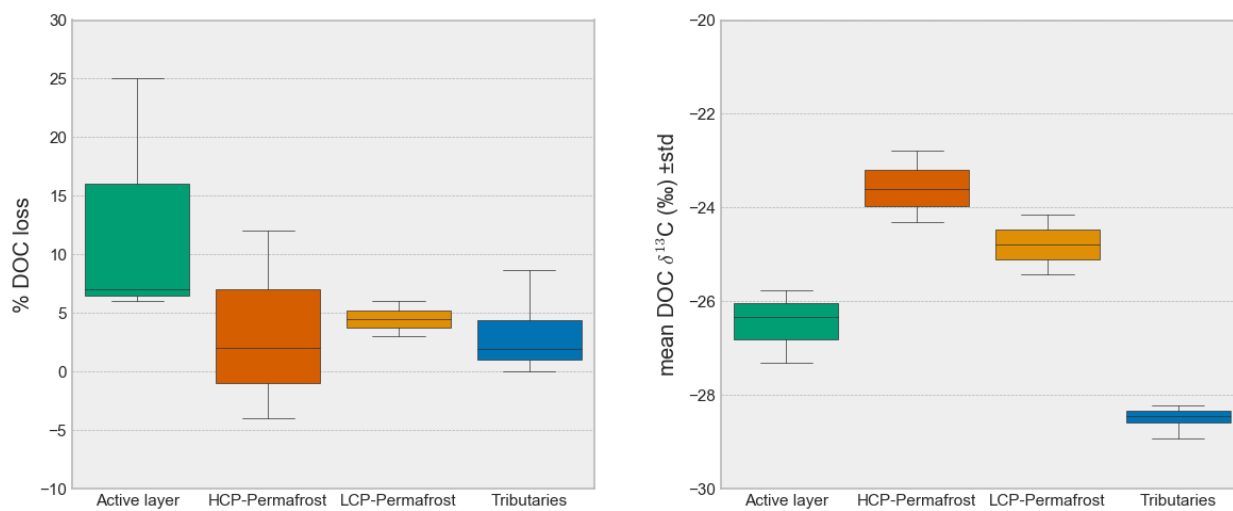


Figure 4. Porewater DOC concentrations (mg/L) across the entire watershed and identified polygon types (HCP, LCP, flat) for permafrost (dark grey box plots) and active layer (light grey) (a), versus depth (b), yield of DOC (in mg) per gram dry soil (c) and yield of DOC (in mg) per gram carbon (d). Color indicates soil organic carbon content (%). Marker type distinguishes soil horizon. Cryoturbated soil samples are annotated with "*" and gleyed soil samples with 'g'.



Main Figures

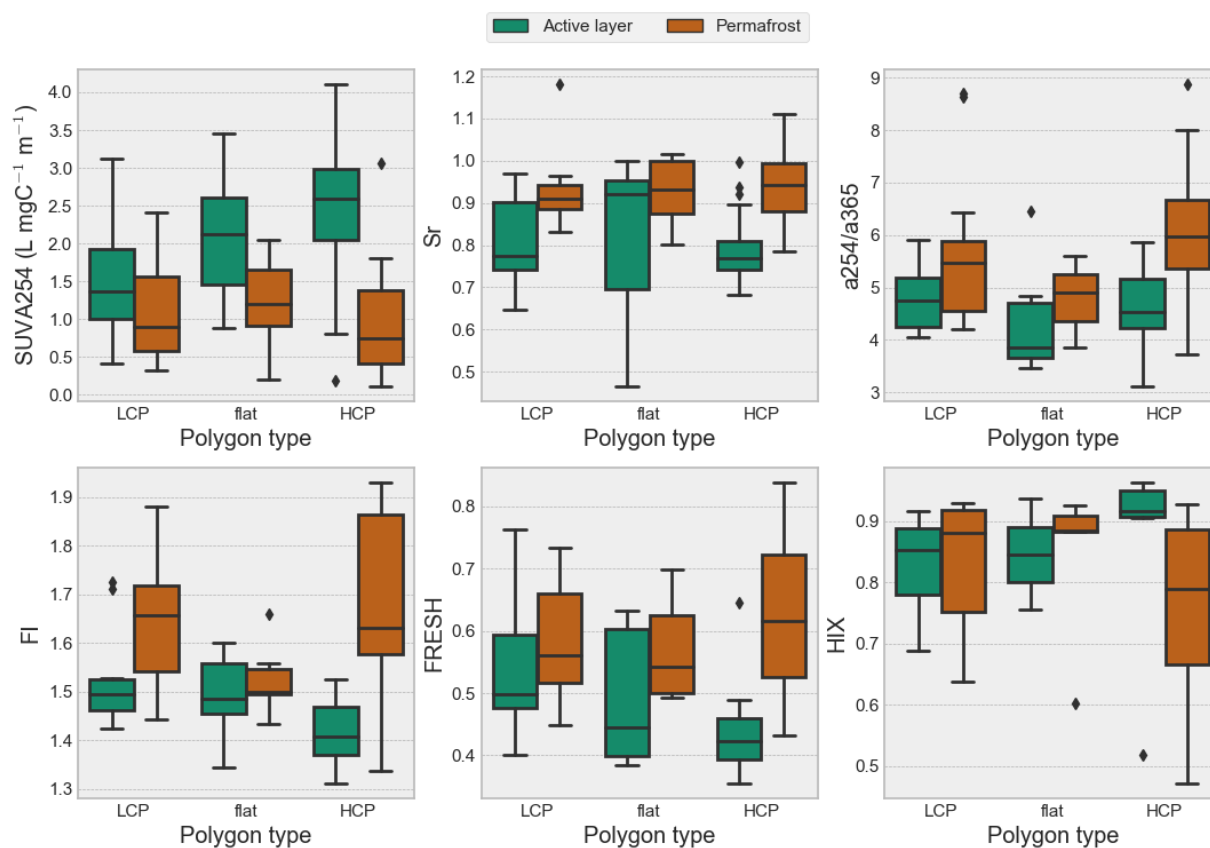


1070

Figure 5. Loss of DOC (%) after 7 days incubation (left), and initial $\delta^{13}\text{C}$ -DOC (right) for the sources active layer (porewater), HCP and LCP permafrost (porewater) and tributaries (stream water).



Main Figures



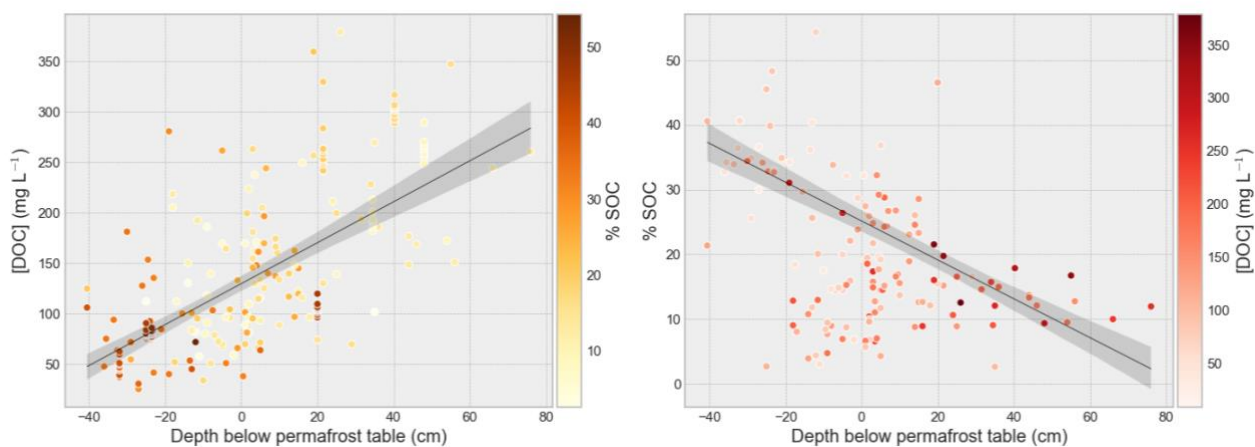
1075

Figure 6. SUVA₂₅₄, slope ratio (Sr), absorbance ratio (a₂₅₄/a₃₆₅), fluorescence index (FI), freshness index (FRESH) and humification index (HIX) for both thermal layers in each polygon type. Differences between the two thermal layers are largest in HCP and smallest in LCP except for FI where flat type polygon has the smallest difference between active layer and permafrost. Indicating a shift in biogeochemical processing of DOM as IWP degradation progresses (i.e. transition from LCP to HCP).



Main Figures

1080



1085

1090

Figure 7. DOC concentration (mg L^{-1}) vs depth to the permafrost table (cm; left panel) and SOC content (% of dry weight) vs depth to the permafrost table (cm; right panel), where negative indicates samples within the active layer and positive below the permafrost table. Colors of the dots show SOC % and DOC concentration respectively, and show the inverse correlation between soil organic carbon content and DOC concentration over the depth of the soil profile. We observe elevated DOC concentrations corresponding with low SOC content around the permafrost table, which may be an effect of flushing in from the overlying Oi-horizons and accumulation above the permafrost table. Linear regression of DOC with depth respective to permafrost table in cm (i.e. active layer depth Z_{AL}) yields $[DOC] = 2.028 \cdot Z_{AL} + 134.60$, $R^2 = 0.71$, $p = 8.6e^{-37}$, for $\%SOC = -0.3 \cdot Z_{AL} + 25.15$, $R^2 = 0.55$, $p = 1.04e^{-19}$.



Main Figures

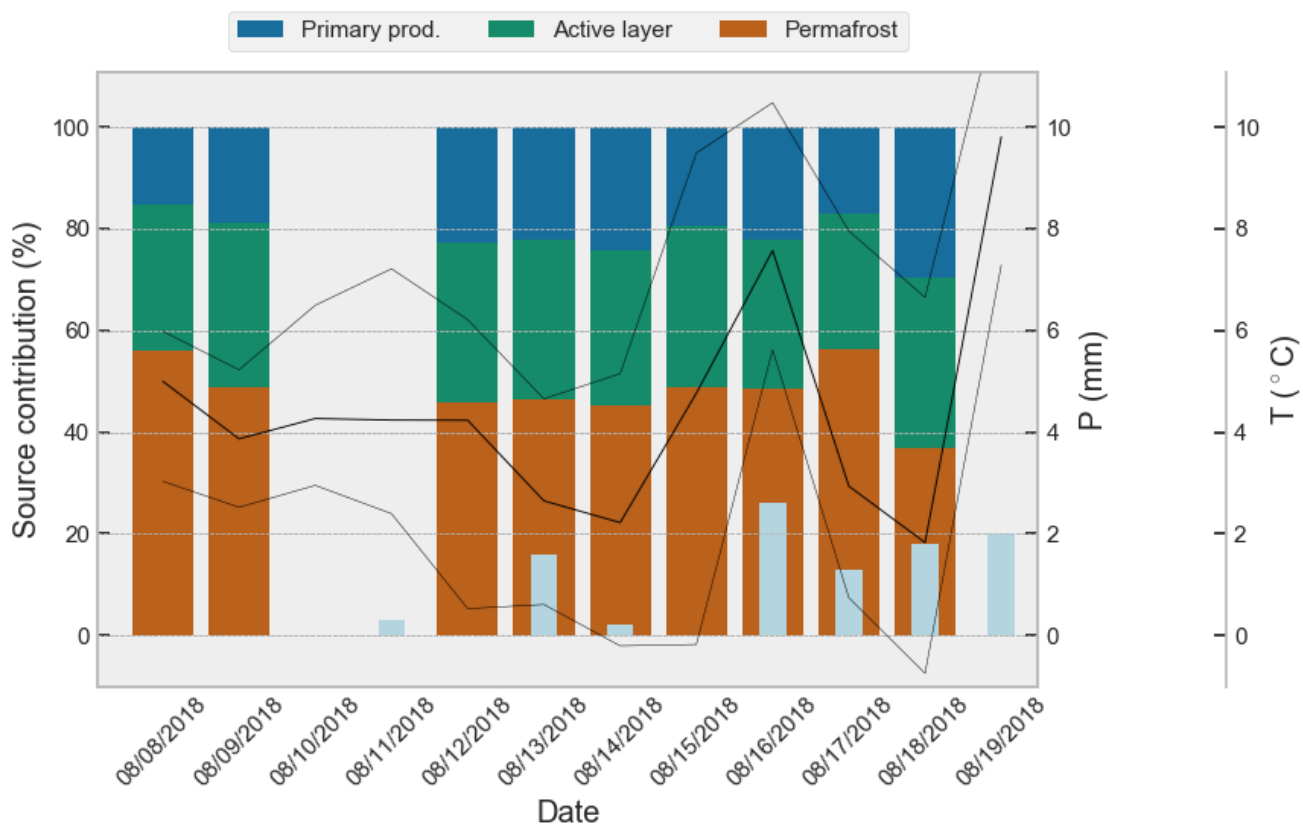


Figure 8. Modeled DOM source contributions, aggregated by day, to catchment outlet sample over time. Plotted together with recorded rainfall (light blue bars) and recorded minimum, maximum and mean air temperature (black lines)

1095



Main Tables

| | | |
|------|--|----|
| | TABLE 1. OVERVIEW OF ABSORBANCE AND FLUORESCENCE INDICES USED | 47 |
| 1100 | TABLE 2. STABLE WATER ISOTOPE VALUES BY SOURCE | 48 |
| | TABLE 3. $\delta^{13}\text{C}$ VALUES OF DOC AND THE POC/SOC DIFFERENT SOURCES | 48 |
| | TABLE 4. CHANGE OF MEAN $\delta^{13}\text{C}$ -DOC BETWEEN THERMAL LAYERS AND POLYGON TYPE | 48 |
| 1105 | TABLE 5. SUMMARY OF FLUORESCENCE AND ABSORBANCE INDICES | 49 |
| | TABLE 6. SOURCE APPORTIONMENT USING $\delta^{13}\text{C}$ -DOC FOR PRIMARY PRODUCTION | 49 |
| 1110 | TABLE 7. SOURCE APPORTIONMENT USING $\delta^{13}\text{C}$ -POC FOR PRIMARY PRODUCTION | 49 |



Main Tables

| Category | Parameter | DOM Indicator | Method |
|---------------------|---|--|---|
| Absorbance | Absorption coefficients (α_{350}) [m^{-1}] | CDOM content | Absorption coefficient at wavelength 350 nm |
| | Absorption ratio | Tracing relative changes in DOM molecular weight (De Haan & De Boer, 1987) | Ratio of absorption coefficients $\alpha_{254}:\alpha_{350}$ [-] |
| | Specific ultraviolet absorbance ($SUVA_{254}$) [$\text{L mg}^{-1} \text{m}^{-1}$] | Aromaticity, $\Delta^{14}\text{C}$ of hydrophobic organic acid (HPOA) fraction of DOC (O'Donnell et al., 2014), $\Delta^{14}\text{C}$ -DOC (Butman et al., 2012) | $SUVA_{254} = \alpha_{254}/[DOC] \cdot 100$ (Weishaar et al., 2003) |
| | Spectral slope ($S_{275-295}$, $S_{350-400}$) [nm^{-1}] and Slope ratio (S_R) [-] | Molecular weight | Nonlinear fit through absorption coefficients between 275–295 nm ($S_{275-295}$), 350–400 nm ($S_{350-400}$) and $S_R = S_{275-295} : S_{350-400}$ |
| Fluorescence | Humification index (HIX) | Indicator of degree of humification or humic substance content (Fellman et al., 2010, Fouché et al., 2017) | The area under the emission spectra 435–480 nm divided by the peak area 300–345 nm + 435–480 nm, at excitation wavelength 254 nm (Ohno, 2002) |
| | Fluorescence index (FI) | Identify relative contribution of terrestrial vs microbial sources (Fouché et al., 2017) | The ratio of emission intensity at wavelength 470 nm and 520 nm, at excitation wavelength 370 nm (McKnight et al., 2001, Cory et al., 2010) |
| | Freshness index ($\beta:\alpha$) | Higher values represent higher proportion of fresh DOM (Fouché et al., 2017) | Emission intensity at 380 nm divided by the maximum emission intensity between 420 nm and 435 nm at excitation 310 nm (Parlanti et al., 2000, Xenopoulos, 2009) |

Table 1. Overview of spectral (absorbance and fluorescence) indices used for DOM qualification.



Main Tables

1115 **Table 2. Stable water isotope values mean and standard deviation by source.**

| Source | $\delta^2\text{H}$ | | $\delta^{18}\text{O}$ | | d-excess | |
|------------------------------|--------------------|------|-----------------------|------|-----------------|------|
| | (mean, std) [‰] | | (mean, std) [‰] | | (mean, std) [‰] | |
| Permafrost porewater (n=18) | -123.3 | ±7.2 | -15.3 | ±1.5 | 1.1 | ±7.6 |
| Active layer porewater (n=8) | -122.6 | ±3.3 | -15.9 | ±0.7 | 4.6 | ±3.3 |
| Tributaries (n=10) | -124.0 | ±2.8 | -16.0 | ±0.4 | 3.9 | ±1.0 |
| Main channel (n=30) | -123.5 | ±8.3 | -15.8 | ±1.1 | 2.5 | ±0.9 |

1120 **Table 3. $\delta^{13}\text{C}$ values of DOC and the POC/SOC for various sources in the catchment. *Note that LCP-active layer $\delta^{13}\text{C}$ -DOC was calculated from the linear relationship between available HCP-active layer $\delta^{13}\text{C}$ -DOC and $\delta^{13}\text{C}$ -SOC and using the $\delta^{13}\text{C}$ -SOC of LCP-active layer. **Values listed are SOC for HCP/LCP active layer and permafrost, and POC for tributaries and main channel.**

| Source | $\delta^{13}\text{C}$ -DOC (mean ±std) | $\delta^{13}\text{C}$ -SOC/POC** (mean ±std) | $\delta^{13}\text{C}$ difference |
|-------------------|--|--|----------------------------------|
| HCP-permafrost | -23.68 ±1.2‰ | -27.35 ±0.8‰ | +3.67‰ |
| LCP-permafrost | -25.05 ±0.5‰ | -27.29 ±1.0‰ | +2.25‰ |
| LCP-active layer* | -26.71 ±1.1‰ | -28.27 ±1.0‰ | +1.56‰ |
| HCP-active layer | -26.38 ±1.1‰ | -27.58 ±0.8‰ | +1.21‰ |
| Tributaries | -28.48 ±0.2‰ | -32.68 ±2.0‰ | +4.21‰ |
| Main channel | -25.40 ±0.4‰ | -29.31 ±0.8‰ | +3.91‰ |

Table 4. Change of mean $\delta^{13}\text{C}$ -DOC (‰ VPDB) between active layer, permafrost for the two polygon types (LCP and HCP).

| Source | $\delta^{13}\text{C}$ -DOC at T ₀ | $\delta^{13}\text{C}$ -DOC at T ₇ | $\delta^{13}\text{C}$ -DOC at T ₂₁ | mean change |
|-------------------------|--|--|---|-------------|
| Active layer (Oi) (n=3) | -26.38 ±1.1‰ | -26.47 ±0.7‰ | -26.22 ±0.8‰ | +0.16‰ |
| LCP-permafrost (n=2) | -25.05 ±0.5‰ | -24.78 ±0.7‰ | -24.89 ±0.6‰ | +0.16‰ |
| HCP-permafrost (n=3) | -23.68 ±1.2‰ | -23.57 ±0.7‰ | -23.59 ±0.8‰ | +0.10‰ |

1125

1130



Main Tables

Table 5. Summary of fluorescence and absorbance indicators of DOM quality. Significant differences and sample sizes are indicated in table S4.

| Index <i>mean ± std</i> | HCP | | LCP | | Flat | | Streams | |
|----------------------------|---------------------|-------------------|---------------------|-------------------|---------------------|-------------------|--------------------|---------------------|
| | <i>Active layer</i> | <i>Permafrost</i> | <i>Active layer</i> | <i>Permafrost</i> | <i>Active layer</i> | <i>Permafrost</i> | <i>Tributaries</i> | <i>Main channel</i> |
| FI | 1.42 ± 0.1 | 1.68 ± 0.2 | 1.53 ± 0.1 | 1.64 ± 0.1 | 1.49 ± 0.1 | 1.52 ± 0.1 | 1.47 ± 0.03 | 1.49 ± 0.02 |
| HIX | 0.86 ± 0.2 | 0.75 ± 0.1 | 0.83 ± 0.1 | 0.83 ± 0.1 | 0.85 ± 0.1 | 0.84 ± 0.1 | 0.96 ± 0.02 | 0.94 ± 0.01 |
| BIX | 0.44 ± 0.1 | 0.64 ± 0.1 | 0.54 ± 0.1 | 0.60 ± 0.1 | 0.50 ± 0.1 | 0.57 ± 0.1 | 0.50 ± 0.04 | 0.56 ± 0.04 |
| FRESH | 0.43 ± 0.1 | 0.62 ± 0.1 | 0.54 ± 0.1 | 0.59 ± 0.1 | 0.49 ± 0.1 | 0.57 ± 0.1 | 0.50 ± 0.04 | 0.56 ± 0.04 |
| a254/a365 | 4.66 ± 0.7 | 6.08 ± 1.1 | 4.81 ± 0.6 | 5.67 ± 1.4 | 4.33 ± 1.4 | 4.80 ± 0.6 | 5.30 ± 0.2 | 5.55 ± 0.3 |
| Sr | 0.79 ± 0.1 | 0.94 ± 0.1 | 0.81 ± 0.1 | 0.92 ± 0.1 | 0.81 ± 0.2 | 0.93 ± 0.1 | 0.80 ± 0.02 | 0.86 ± 0.03 |
| SUVA ₂₅₄ | 2.42 ± 0.9 | 0.91 ± 0.7 | 1.50 ± 0.8 | 1.10 ± 0.7 | 2.09 ± 0.9 | 1.23 ± 0.6 | 3.86 ± 1.8 | 3.90 ± 2.2 |

Table 6. Mean relative contribution of three identified sources (source fractions) to the integrated signal at the catchment outlet, using $\delta^{13}\text{C}$ -DOC for the primary production endmember.

| Source | 2.5% percentile | median | 97.5% percentile | mean | Std. |
|--------------------|-----------------|--------|------------------|-------|------|
| Permafrost | 0.075 | 0.488 | 0.830 | 0.479 | 0.19 |
| Active layer | 0.013 | 0.271 | 0.788 | 0.305 | 0.21 |
| Primary production | 0.015 | 0.192 | 0.561 | 0.216 | 0.15 |

Table 7. Mean relative contribution of three identified sources (source fractions) to the integrated signal at the catchment outlet, using $\delta^{13}\text{C}$ -POC for the primary production endmember.

| Source | 2.5% percentile | median | 97.5% percentile | mean | Std. |
|--------------------|-----------------|--------|------------------|-------|------|
| Permafrost | 0.124 | 0.564 | 0.872 | 0.545 | 0.19 |
| Active layer | 0.025 | 0.315 | 0.808 | 0.341 | 0.22 |
| Primary production | 0.006 | 0.095 | 0.329 | 0.114 | 0.09 |